Commun Nonlinear Sci Numer Simulat 67 (2019) 124–151

Contents lists available at ScienceDirect

Commun Nonlinear Sci Numer Simulat

journal homepage: www.elsevier.com/locate/cnsns

Research paper

A novel homotopy-wavelet approach for solving stream function-vorticity formulation of Navier–Stokes equations

Qiang Yu, Hang Xu*, Shijun Liao, Zhaochen Yang

Collaborative Innovation Center for Advanced Ship and Deep-Sea Exploration (CISSE) State Key Laboratory of Ocean Engineering, School of Naval Architecture Ocean and Civil Engineering Shanghai Jiao Tong University, Shanghai 200240, China

ARTICLE INFO

Article history:
Received 13 July 2017
Revised 2 June 2018
Accepted 1 July 2018
Available online 10 July 2018

Keywords:
Nonhomogeneous boundaries
Cavity flow
High efficiency computation
Homotopy-wavelet

ABSTRACT

In this paper, we propose a new homotopy-wavelet approach to solve linear and nonlinear problems with nonhomogeneous boundary conditions. The essence of this technique is to apply the homotopy analysis method (HAM) to transform the governing equations into a set of linear equations and employ the generalized Coiflet-type orthogonal wavelet to express and solve the resulting linear equations. The proposed technique is expected to keep the superiority of the HAM for handling nonlinearities, but with better computational efficiency. The nonhomogeneous boundary conditions including the mixed Dirichlet-Neumann and Robin conditions are reconstructed by introducing the Coiflets on the boundaries, which overcomes the deficiency of the close wavelet method that is difficult to handle the nonhomogeneous boundary conditions. Illustrative examples show very high efficiency of our proposed technique. Furthermore, the classic problem of the incompressible flow in a 2-D lid-driven cavity are investigated. By reconstructing the incompatible boundary conditions with the Coiflets, the singularities of velocity field on rigid points are successfully eliminated so that the vortex on the lid that is difficult to be obtained by previous approaches can be captured clearly. Comparison with previous results is made, excellent agreement is found.

© 2018 Elsevier B.V. All rights reserved.

1. Introduction

In the past several decades, wavelet analysis [1] has been developed as a very efficient analytical tool to give solutions for various kinds of differential equations. The classic Daubechies wavelets were commonly used as the classical compactly supported wavelet to resolve boundary value problems for a long time. To improve on solution accuracy via enlarging the wavelet supported branch, Coifman [2] established Coiflets wavelet which possesses the property that both scaling and wavelet functions have vanishing moment whose support region is three times over the biggest vanishing moment. Since then, Coiflets wavelet received considerable attention and was successively developed by many researchers. For examples, Sweldens [3] and Tian [4] respectively proposed the standard orthogonal and the biorthogonal Coiflets systems which were shown to be accurate for wavelet approximations in graphical optimization algorithm. Wei [5] generalized the orthogonal and biorthogonal Coiflets by modifying conditions of moments of scaling functions. Zhang et al. [6], Wang [7] and Liu et al. [8] further suggested a closed wavelet method based on the generalized orthogonal Coiflets system (GOCS), which is expected to give more accurate solutions by enlarging the first order vanishing moment from 6 to 7. Generally speaking,

* Corresponding author.
E-mail addresses: jsslsxyq@sjtu.edu.cn (Q. Yu), hangxu@sjtu.edu.cn (H. Xu), sjliao@sjtu.edu.cn (S. Liao), zcyang872@sjtu.edu.cn (Z. Yang).

https://doi.org/10.1016/j.cnsns.2018.07.001
1007-5704/© 2018 Elsevier B.V. All rights reserved.

the basic approach for construction of the Coiflets is the boundary modification [9], that means building interpolation functions based on the boundary point for extension. The boundary interpolation matrices are modified in accordance with homogeneous conditions. Variable and nonlinear parts are then approximated by different wavelets respectively. In this way, nonlinear differential equations can be transformed into nonlinear algebra ones. Coefficients of Coiflets series are finally determined by the Newton iterating method.

Though many nonlinear problems have been attacked by a number of wavelet users, few of them [10,11] considered nonhomogeneous nonlinear problems widely appeared in the fields of science and engineering. For such problems, they usually homogenize the boundary conditions by introducing proper auxiliary functions, then solve the differential equations with their homogenous boundary conditions by above-mentioned closed wavelet method. Unfortunately, two major issues are usually encountered in this approach.

- For 1-D nonhomogeneous problems, though the boundary conditions can be normalized, it is extremely difficult to choose an optimal auxiliary homogeneous function to reduce loss of the approaching precision of wavelet solutions owing to the non-uniqueness of the selected function.
- For 2-D or 3-D problems, it is almost impossible to find such an appropriate auxiliary function to normalize the boundary conditions, which can hardly be resolved by previous wavelet techniques.

Obviously, it is very urgent to extend the existing wavelet technique so that the nonhomogeneous problems can be readily resolved by this technique.

In this study, nonlinear problems with nonhomogeneous boundary conditions including Dirichlet, Neumann and Robin types' boundaries will be investigated in-depth. Based on the former work [12–14], the nonhomogeneous boundaries will be handled by a novel wavelet technique based on the modification of the Coiflets via introducing a spline function of polynomial type that possesses the nonhomogeneous behaviours on the boundaries. we combine the Coiflets basis with the Homotopy Analysis Method (HAM) [15–21] for solving those problems. By selecting proper linear operators, optimal convergence-control parameters and completeness auxiliary functions, the original nonlinear differential equation is converted into an infinity number of linear differential equations. Solutions of those linear equations are approximated by wavelets and obtained by Wavelet–Galerkin method which is applied to transform those linear differential equations to linear algebra ones by means of the Generalized Gauss Integration Method [22].

The paper is outlined as follows. In Section 2, boundary wavelets are introduced. In Section 3, the validity and efficiency of this approach is checked by examining 1-D and 2-D nonhomogeneous partial differential equations governed by the Laplace and the Biharmonic operators respectively. In Section 4, the classical lid driven cavity flow subjected to mixed Neumann-Dirichlet boundary in two cases that the up lid moves in variable velocity with analytical solution and in a constant velocity with unknown analytical solution are investigated as an illustrative example in comparison with other numerical results. In Section 5, some conclusions are made.

2. Boundary modification by the generalized orthogonal Coiflets

The boundary zero extension is often encountered when a function of finite interval is approximated by the compactly supported wavelet basis. It can increase errors in approaching process since the continuous and non-derivative points on edge result in Gibbs's border jump.

In order to improve on the approaching precision, the interpolated extension [8] by the Taylor expansions for $f(x)$ at $x = 0$ and $x = 1$ are conducted respectively.

$$\widetilde{f}(x) = \begin{cases} \sum_{k=0}^{3} f_{j,k} T_{0,k}(x), x \in (-\delta, 0), \\ f(x), \quad x \in [0, 1], \\ \sum_{k=0}^{3} f_{j,2^j-k} T_{1,k}(x), x \in (1, 1+\delta). \end{cases} \tag{1}$$

where δ is small amount, j is wavelet resolution level, $T_{0,k}(x)$ and $T_{1,k}(x)$ are the modification functions defined by

$$T_{0,k}(x) = \sum_{i=0}^{3} \left(\frac{p_{i,k}^0}{i!} \right) x^i, \quad T_{1,k}(x) = \sum_{i=0}^{3} \left(\frac{p_{i,k}^1}{i!} \right) (x-1)^i. \tag{2}$$

with $p_{i,k}^0$ and $p_{i,k}^1$ determined by coefficients matrices $\mathbf{P}_0$ and $\mathbf{P}_1$.

$$\mathbf{P_0} = \begin{pmatrix} 1 & 0 & 0 & 0 \\ -11/6 & 3 & -3/2 & 1/3 \\ 2 & -5 & 4 & -1 \\ -1 & 3 & -3 & 1 \end{pmatrix}, \quad \mathbf{P_1} = \begin{pmatrix} 1 & 0 & 0 & 0 \\ 11/6 & -3 & 3/2 & -1/3 \\ 2 & -5 & 4 & -1 \\ 1 & -3 & 3 & -1 \end{pmatrix}.$$

Taking the compactly supported region of wavelets [0, L] and the domain of function [0,1] into consideration [7], $\widetilde{f}(x)$ is approximated as

$$\widetilde{f}(x) \approx \sum_{k=2-3N}^{2^j-1} \widetilde{f}\left(\frac{M_1 + k}{2^j} \right) \phi(2^j x - k) = \sum_{k=2-3N+M_1}^{2^j-1+M_1} \widetilde{f}\left(\frac{k}{2^j} \right) \phi(2^j x - k + M_1). \tag{3}$$

where M_1 is the first order vanishing moment, N is the vanishing moment, L is the compactly supported length which equates to $3N-1$ in Coiflets family, ψ is the wavelet basis. It turns out that the coefficients of Coiflets series are the approximate values of the middle points of the function.

The essence of the above-mentioned closed wavelet method is the polynomial interpolation by three points at $x=0$ and $x=1$. However, when the boundary conditions are not homogeneous, this approach is invalidate since the information of the variables and their derivatives on the boundaries can not be kept properly by the Coiflets. To overcome this limitation, we construct the following spline function by including additional functions of polynomial types on the boundaries into the Coiflets, which hold all inhomogeneous behaviours of the solutions.

$$\hat{f}(x)=\begin{cases}\sum_{k=0}^{3}\left[f_{j,k}T_{0,k}(x)+\frac{\alpha_{0,k}}{k!}x^k\right], & x\in(-\delta,0),\\ f(x), & x\in[0,1],\\ \sum_{k=0}^{3}\left[f_{j,2^j-k}T_{1,k}(x)+\frac{\alpha_{1,k}}{k!}(x-1)^k\right], & x\in(1,1+\delta).\end{cases}\tag{4}$$

Substituting Eq. (4) into Eq. (3), we obtain

$$\tilde{f}(x)=\begin{cases}\sum_{k=0}^{3}f_{j,k}\left\{\sum_{i=2-3N+M_1}^{-1}T_{0,k}\left(\frac{i}{2^j}\right)\phi_{j,i}+\phi_{j,k}\right\}\\ +\sum_{k=0}^{3}\frac{\alpha_{0,k}}{k!}\left\{\sum_{i=2-3N+M_1}^{-1}\left(\frac{i}{2^j}\right)^k\phi(2^jx-i+M_1)\right\} & k\in[0,3],\\ \sum_{k=4}^{2^j-4}f_{j,k}\phi_{j,k} & k\in[4,2^j-4],\\ \sum_{k=2^j-3}^{2^j}f_{j,k}\left\{\sum_{i=2^j+1}^{2^j-1+M_1}T_{1,2^j-k}\left(\frac{i}{2^j}\right)\phi_{j,i}+\phi_{j,k}\right\}\\ +\sum_{k=0}^{3}\frac{\alpha_{1,k}}{k!}\left\{\sum_{i=2^j+1}^{2^j-1+M_1}\left(\frac{i}{2^j}-1\right)^k\phi(2^jx-i+M_1)\right\} & k\in[2^j-3,2^j],\end{cases}\tag{5}$$

where

$$\phi_{j,i}=\phi(2^jx-i+M_1),\quad \phi_{j,k}=\phi(2^jx-k+M_1).$$

Taking Eq. (5) into account, the targeted approximation of $\tilde{f}(x)$ is divided into two parts. One is the generalized Coiflets [8] with the polynomial interpolation modifications on the boundaries

$$\varphi_{j,k}(x)=\begin{cases}\sum_{i=2-3N+M_1}^{-1}T_{0,k}\left(\frac{i}{2^j}\right)\phi_{j,i}+\phi_{j,k} & k\in[0,3],\\ \sum_{k=4}^{2^j-4}\phi_{j,k} & k\in[4,2^j-4],\\ \sum_{i=2^j+1}^{2^j-1+M_1}T_{1,2^j-k}\left(\frac{i}{2^j}\right)\phi_{j,i}+\phi_{j,k} & k\in[2^j-3,2^j].\end{cases}\tag{6}$$

The other is the boundary wavelets, which are expressed by

$$\varpi_{j,a}^{0}(x)=\sum_{i=2-3N+M_1}^{-1}\frac{1}{a!}\left(\frac{i}{2^j}\right)^a\phi_{j,i},\quad \varpi_{j,b}^{1}(x)=\sum_{i=2^j+1}^{2^j-1+M_1}\frac{1}{b!}\left(\frac{i}{2^j}-1\right)^b\phi_{j,i}.\tag{7}$$

where the prefix 0,1 correspond to the left and right boundaries and suffix *a, b* related to orders respectively.

3. Application in linear cases

3.1. Wavelet expansion for various boundary conditions

We then make attempts to apply the above-mentioned modified generalized orthogonal Coiflets to solve linear problems subjected to the boundary conditions of Dirichlet, Neumann and Robins' types, respectively. The strategy is elaborated as follows.

For a linear equation

$$\mathcal{L}[u(x)]=0.\tag{8}$$

its boundary conditions can be expanded by Coiflets, upon the type of the boundary conditions, into the following forms:

- Dirichlet boundary condition

$$u(0)=C_0,\quad u(1)=C_1.\tag{9}$$

It should be noted that such boundary conditions can be handled directly by the traditional wavelet expansion (refer to Wang [7]) as

$$u(x)\approx P^ju(x)=\sum_{k=1}^{2^j-1}u\left(\frac{k}{2^j}\right)\varphi_{j,k}(x)+C_0\varphi_{j,0}(x)+C_1\varphi_{j,2^j}(x).\tag{10}$$

- Neumann boundary condition

$$\left.\frac{\mathrm{d}^{\mathrm{a}}\mathrm{u}(\mathrm{x})}{\mathrm{dx}^{\mathrm{a}}}\right|_{x=0}=C_0,\quad \left.\frac{\mathrm{d}^{\mathrm{b}}\mathrm{u}(\mathrm{x})}{\mathrm{dx}^{\mathrm{b}}}\right|_{x=1}=C_1. \tag{11}$$

In literature, Wang [7] constructed the following wavelet to solve differential equations with Neumann boundary conditions. While his approach is only valid for the homogeneous boundary conditions ($C_0=C_1=0$).

$$h_{j,k}(x)=\varphi_{j,k}(x)|_{p_{0,a,i}\to 0,\,p_{1,b,i}\to 0}. \tag{12}$$

For non-homogeneous boundary conditions, we construct the following boundary wavelet

$$u(x)\approx P^j u(x)=\sum_{k=0}^{2^j} u\left(\frac{k}{2^j}\right)h_{j,k}(x)+C_0\varpi_{j,a}^0(x)+C_1\varpi_{j,b}^1(x). \tag{13}$$

- Robin boundary condition

As far as we know, few researchers considered such boundary conditions before. On the boundaries, the following relationship can be built

$$\left.\frac{\mathrm{d}^{\mathrm{a}}\mathrm{u}(\mathrm{x})}{\mathrm{dx}^{\mathrm{a}}}+k_1u(x)\right|_{x=0}=C_0,\quad \left.\frac{\mathrm{d}^{\mathrm{b}}\mathrm{u}(\mathrm{x})}{\mathrm{dx}^{\mathrm{b}}}+k_2u(x)\right|_{x=1}=C_1. \tag{14}$$

By modifying the interpolation functions $T_{0,\,k}$ and $T_{1,\,k}$, we obtain

$$\tilde{T}_{0,k}=\begin{cases}T_{0,k}-k_1\frac{x^a}{a!}, & k=0,\\ T_{0,k}, & k>0.\end{cases} \tag{15}$$

and

$$\tilde{T}_{1,k}=\begin{cases}T_{1,k}-k_2\frac{(x-1)^b}{b!}, & k=0,\\ T_{1,k}, & k>0.\end{cases} \tag{16}$$

Finally, we obtain the wavelet approximation for $u(x)$ as

$$u(x)\approx P^j u(x)=\sum_{k=0}^{2^j} u\left(\frac{k}{2^j}\right)h_{j,k}(x)+C_0\varpi_{j,a}^0(x)+C_1\varpi_{j,b}^1(x), \tag{17}$$

where

$$h_{j,k}(x)=\varphi_{j,k}(x)|_{p_{0,a,i}\to 0,\,p_{1,b,i}\to 0,\,T_{0,k}\to\tilde{T}_{0,k},\,T_{1,k}\to\tilde{T}_{1,k}}. \tag{18}$$

3.2. Validation in 1-D linear cases

In this section, we will now present two examples in 1-D cases, aimed to validate the method in terms of accuracy and assess its performance. For nonhomogeneous problems, Liu et al. [8] chose auxiliary functions of polynomial type to homogenize them, then applied the Wavelet-Galerkin method to solve the resulting homogeneous ones. However, this approach is only valid for differential equations with Dirichlet boundary conditions. Different from what Liu et al. [8] did, we directly approximate variables by Coiflets together with the boundary wavelets, without homogenizing them by auxiliary functions. Our examples are shown in details thereinafter.

In order to estimate error distribution in 1D case, criterion $Err(x)$ between calculated results $u(x)$ and exact solutions $u_e(x)$ using the Norm-1 of $\mathbf{L}^2[0,\,1]$,

$$Err(x)=\left|u(x)-u_e(x)\right|,\quad 0<x<1. \tag{19}$$

To illustrate the global error level, more consideration of *ErrSQ* vanishing to zero is essential in contrast with exact or numerical solutions while exact ones are non-existent. Numerical integration of Norm-2 in $\mathbf{L}^2[0,\,1]$ is

$$ErrSQ=||Err(x)||^2_{\mathbf{L}^2[0,1]}\approx\frac{1}{(2^j+1)}\sum_{k=0}^{2^j}\left[u\left(\frac{k}{2^j}\right)-u_e\left(\frac{k}{2^j}\right)\right]^2. \tag{20}$$

We first consider the 1-D linear differential equation

$$\frac{\mathrm{d}^2u(x)}{\mathrm{d}x^2}-2\pi\frac{\mathrm{d}u(x)}{\mathrm{d}x}+2\pi^2u(x)=0. \tag{21}$$

subjected to the Neumann boundary conditions

$$u'(0)=e^{-\pi},\quad u'(1)=-1. \tag{22}$$

with the analytical solution

$$u_e(x) = \frac{1}{\pi} e^{\pi(x-1)} \sin \pi x. \tag{23}$$

Using Liu's approach [8], $u(x)$ can be expressed by

$$u(x) = w(x) + v(x). \tag{24}$$

subjected to

$$w'(0) = 0, \quad w'(1) = 0, \quad v'(0) = e^{-\pi}, \quad v'(1) = -1. \tag{25}$$

where $w(x)$ is the homogenized function to be determined, $v(x)$ is the auxiliary homogeneous function that is known and holds the information of the boundaries.

Substituting Eq. (24) into Eq. (21), we obtain

$$\frac{\mathrm{d}^2 w}{\mathrm{d}x^2} - 2\pi \frac{\mathrm{d}w}{\mathrm{d}x} + 2\pi^2 w = -\mathcal{L}[v(x)], \tag{26}$$

where

$$\mathcal{L} = \frac{\mathrm{d}^2}{\mathrm{d}x^2} - 2\pi \frac{\mathrm{d}}{\mathrm{d}x} + 2\pi^2. \tag{27}$$

It is known that $v(x)$ is not unique, which can have many different forms. For example, we can select

$$v(x) = e^{-\pi} x - (e^{-\pi} + 1) \frac{x^K}{K}, \tag{28}$$

where $K \geq 2$ is the integer.

The wavelet approximations for $w(x)$ and $v(x)$ can be written by different wavelet basis as

$$w(x) \approx \sum_{k=0}^{2^j} u\left(\frac{k}{2^j}\right) h_{j,k}(x), \quad \mathcal{L}[v(x)] \approx \sum_{k=0}^{2^j} \mathcal{L}\left[v\left(\frac{k}{2^j}\right)\right] \varphi_{j,k}(x). \tag{29}$$

where

$$h_{j,k}(x) = \varphi_{j,k}(x)|_{p_{0,1,i} \to 0, p_{1,1,i} \to 0,} \tag{30}$$

According the General Gaussian Integration Method(GGIM) [22], the linear operator $\mathcal{L}$ and the nonlinear operator $\mathcal{N}$ acting on the wavelet approximate functions can be transformed to the following forms

$$\mathcal{R}[\widetilde{f}(x)] \approx \mathcal{R}[P^j \widetilde{f}(x)] = \sum_{2-3N+M_1}^{2^j-1+M_1} \widetilde{f}\left(\frac{k}{2^j}\right) \mathcal{R}[\phi_{j,k}(x)], \quad \mathcal{R} = \mathcal{L}, \mathcal{N}. \tag{31}$$

Some symbolic definitions can be referred in Appendix A. By multiplying $h_{j,l}(x)$ on both sides of Eq. (31) and then integrating on the interval [0,1], we obtain

$$\tilde{\mathbf{A}}_1 \bullet \hat{\mathbf{U}}_1 + \tilde{\mathbf{B}}_1 \bullet \hat{\mathbf{V}}_1 = \mathbf{0}. \tag{32}$$

where straight vectors are

$$\hat{\mathbf{U}}_1 = \left\{u_k = u\left(\frac{k}{2^j}\right)\right\}, \quad \tilde{\mathbf{A}}_1^T = \mathbf{\Gamma}_{k,l}^{j,2} - 2\pi \mathbf{\Gamma}_{k,l}^{j,1} + 2\pi^2 \mathbf{\Gamma}_{k,l}^{j,0},$$

$$\tilde{\mathbf{B}}_1^T = \bar{\mathbf{\Gamma}}_{k,l}^{j,0}, \quad \hat{\mathbf{V}}_1 = \left\{v_k = \mathcal{L}\left[v\left(\frac{k}{2^j}\right)\right]\right\}.$$

in which, the tensors of connection coefficients are given by

$$\mathbf{\Gamma}_{k,l}^{j,n} = \left\{\gamma_{k,l}^{j,n} = \int_0^1 \frac{d^n h_{j,k}(x)}{dx^n} h_{j,l}(x) dx\right\}, \tag{33}$$

$$\bar{\mathbf{\Gamma}}_{k,l}^{j,n} = \left\{\bar{\gamma}_{k,l}^{j,n} = \int_0^1 \frac{d^n \varphi_{j,l}(x)}{dx^n} h_{j,k}(x) dx\right\}. \tag{34}$$

Different from Liu's approach [8], We directly expand $u(x)$, without introducing homogeneous function, as

$$u(x) \approx P^j u(x) = \sum_{k=0}^{2^j} u\left(\frac{k}{2^j}\right) h_{j,k}(x) + e^{-\pi} \varpi_{j,L}(x) - \varpi_{j,R}(x), \tag{35}$$

by setting

$$\varpi_{j,L}(x) = \varpi_{j,1}^0(x), \quad \varpi_{j,R} = \varpi_{j,1}^1(x). \tag{36}$$

Table 1
The consuming CPU time and precisions $ErrSQ_u$ for 1-D linear problem subjected to the Neumann and the mixed Dirichlet-Neumann boundary conditions.

Boundary types	j	3	4	5	6
Neumann	$ErrSQ_u$	7.969E−03	4.195E−04	4.094E−05	7.164E−07
Neumann	CPU time(s)	1.805	2.258	3.087	6.090
Mixed	$ErrSQ_u$	3.617E−07	3.051E−09	1.710E−11	9.548E−14
Mixed	CPU time(s)	1.454	1.546	2.531	5.485

Multiplying $h_{j,l}(x)$ on both sides and then applying the Wavelet–Galerkin Method, we obtain

$$\tilde{\mathbf{A}}_1 \bullet \hat{\mathbf{U}}_1 + e^{-\pi}\tilde{\mathbf{B}}_L - \tilde{\mathbf{B}}_R = \mathbf{0}. \tag{37}$$

where

$$\tilde{\mathbf{B}}_i^T = \hat{\mathbf{\Gamma}}_{i,l}^{j,2} - 2\pi\hat{\mathbf{\Gamma}}_{i,l}^{j,1} + 2\pi^2\hat{\mathbf{\Gamma}}_{i,l}^{j,0}, \quad i = L, R.$$

here the connection coefficients determined by sides and orders of boundary derivatives where the first subscript 0,1 represent the derivatives in integration with order n are

$$\hat{\mathbf{\Gamma}}_{L,k}^{j,n} = \left\{\bar{\gamma}_{L,k}^{j,n} = \int_0^1 \frac{d^n\varpi_{j,L}(x)}{dx^n}h_{j,k}(x)dx\right\},$$
$$\hat{\mathbf{\Gamma}}_{R,k}^{j,n} = \left\{\bar{\gamma}_{R,k}^{j,n} = \int_0^1 \frac{d^n\varpi_{j,R}(x)}{dx^n}h_{j,k}(x)dx\right\}. \tag{38}$$

Further to check the validity of our approach, we consider Eq. (27) subjected to the Neumann and the mixed Dirichlet–Neumann boundary conditions. In this case, the boundary conditions take the form

$$u(0) = 0, \quad u'(1) = -1. \tag{39}$$

The auxiliary function $v(x)$ for Liu's approach [8] is replaced by

$$v(x) = -\frac{x^K}{K}, \quad K \geq 2, K \in Z. \tag{40}$$

Our wavelet extension for $u(x)$ is

$$u(x) \approx \sum_{k=1}^{2^j} u\left(\frac{k}{2^j}\right)h_{j,k}(x) - \varphi_{j,1}^1(x). \tag{41}$$

Using the software Mathematica on an ordinary laptop (CPU Intel Core i7-6500U 2.5 GHz, Memory 8GB), it is readily to give results for those equations. As shown in Table 1, our approach can give excellent results in very short time. We notice that the precision of wavelet solutions improves gradually as the resolution level j increases. Note that the homogeneous auxiliary function introduced by Liu et al. [8] is non-unique, which leads to the computational accuracies could be seriously affected when this function is changed, as shown in Fig. 1. Particularly, for the mixed Dirichlet-Neumann boundary conditions' case, it is found that when $K = 4$, the square error of Liu's [8] can reach 1.0×10^{-14} in about five seconds. Unfortunately, it is not easy to find this optimal value K, a series of computations are needed for determination of this best value. The total time consumed in the computation is therefore very much. Without taking efforts to try the best value of the optimal parameter K, we are able to obtain the exact wavelet approximations directly by our approach, the errors can readily reach to 9.54866×10^{-14} in very short time, as shown in Fig. 2 (Dash red line). This shows great priority of our proposed technique.

3.3. Validation in 2-D linear cases

Further to verify the validity and efficiency of our proposed approach, we apply it in the nonhomogeneous 2-D linear problem. Note that for such case, Liu's approach [8] can hardly find an appropriate auxiliary function to homogenize the nonhomogeneous boundaries. This is to say, his approach is invalid for most 2-D problems with the nonhomogeneous boundaries. While our skill still work very well, as illustrated below.

The governing equation considered here is in the following form

$$\mathcal{L}[\xi(x, y)] = 0, \tag{42}$$

subjected to the boundary conditions

$$\left.\frac{\partial^a\xi}{\partial x^a}\right|_{x=0} = f_1(y), \quad \left.\frac{\partial^b\xi}{\partial x^b}\right|_{x=1} = f_2(y),$$
$$\left.\frac{\partial^c\xi}{\partial y^c}\right|_{y=0} = g_1(x), \quad \left.\frac{\partial^d\xi}{\partial y^d}\right|_{y=1} = g_2(x). \tag{43}$$

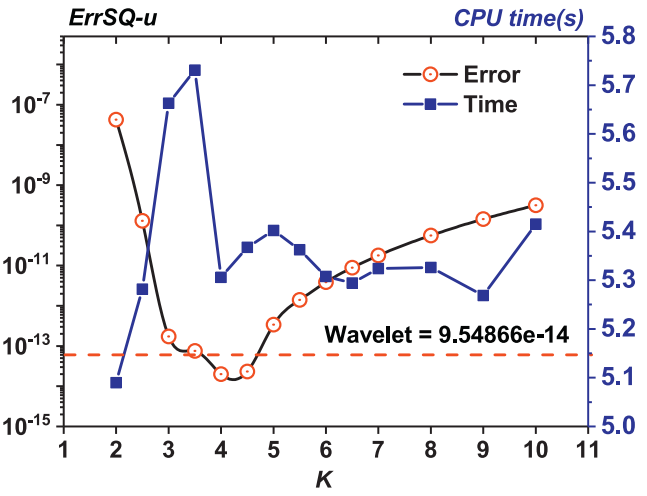

Fig. 1. Approaching precision and consuming time of auxiliary function with different order K by Liu's approach. $ErrSQ-u$: solid with rectangular points; CPU time: solid with circle points; Red dash horizontal line: approaching precision of our approach with boundary Coiflets. (For interpretation of the references to color in this figure legend, the reader is referred to the web version of this article.)

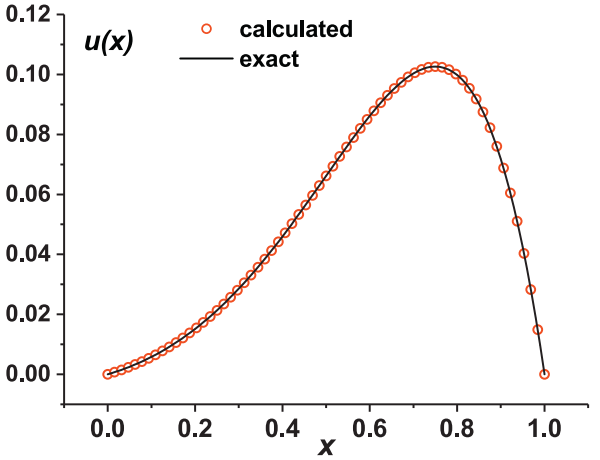

Fig. 2. Comparison in 1-D case subjected to the mixed Dirichlet-Neumann boundary. Calculated results ($j = 6$): red circled points; exact solution: black line. (For interpretation of the references to colour in this figure legend, the reader is referred to the web version of this article.)

where a, b, c, d are orders of function on the left side $x = 0$, the right side $x = 1$, the down side $y = 0$ and the up side $y = 1$, respectively.

Using our approach, the boundary interpolation matrices can be modified as

$$h_{j,k}(x) = \varphi_{j,k}(x)|_{p_{0,a,i}\to 0, p_{1,b,i}\to 0,} \quad h_{j,l}(y) = \varphi_{j,l}(y)|_{p_{0,c,i}\to 0, p_{1,d,i}\to 0.} \tag{44}$$

So that the wavelet approximations can be written by

$$\xi(x,y) \approx P^j\xi(x,y) = \sum_{k=0}^{2^j}\sum_{l=0}^{2^j}\xi\left(\frac{k}{2^j},\frac{l}{2^j}\right)h_{j,k}(x)h_{j,l}(y) + B_\xi^n, \tag{45}$$

where modification by nonhomogeneous boundary are

$$B_\xi^n = h_{j,k}(x)\left\{\sum_{k=0}^{2^j} g_1\left(\frac{k}{2^j}\right)\varpi_{j,c}^0(y) + \sum_{k=0}^{2^j} g_2\left(\frac{k}{2^j}\right)\varpi_{j,d}^1(y)\right\}$$

$$+h_{j,l}(y)\left\{\sum_{l=0}^{2^j} f_1\left(\frac{l}{2^j}\right)\varpi_{j,a}^0(x) + \sum_{l=0}^{2^j} f_2\left(\frac{l}{2^j}\right)\varphi_{j,b}^1(x)\right\}.$$

Analogous to Eqs. (19) and (20), the distributed error function and system errors for 2D case are defined as

$$Err_\xi(x,y) = \left|\xi(x,y) - \xi_e(x,y)\right|^2, \quad 0 < x, y < 1, \tag{46}$$

$$ErrSQ_{\xi} \approx \frac{1}{(2^j+1)^2}\sum_{k=0}^{2^j}\sum_{l=0}^{2^j}\left[\xi\left(\frac{k}{2^j},\frac{l}{2^j}\right)-\xi_e\left(\frac{k}{2^j},\frac{l}{2^j}\right)\right]^2. \tag{47}$$

where $\xi(x, y)$ and $\xi_e(x, y)$ are the wavelet approximation and the analytical solution, respectively.

The first example for the 2-D linear equation governed by Laplace operator is given by

$$\Delta\xi+\pi^2\xi+f=0,\quad f=\pi^2(\bar{M}^2+\bar{N}^2-1)\sin(\bar{M}\pi x)\sin(\bar{N}\pi y), \tag{48}$$

with the analytical solution

$$\xi_e(x,y)=\sin(\bar{M}\pi x)\sin(\bar{N}\pi y). \tag{49}$$

subjected to Neumann type boundary conditions

$$\begin{aligned}&\left.\frac{\partial\xi}{\partial x}\right|_{x=0}=\bar{M}\pi\sin(\bar{N}\pi y),\quad \left.\frac{\partial\xi}{\partial x}\right|_{x=1}=(-1)^{\bar{M}}\bar{M}\pi\sin(\bar{N}\pi y),\\ &\left.\frac{\partial\xi}{\partial y}\right|_{y=0}=\bar{N}\pi\sin(\bar{M}\pi x),\quad \left.\frac{\partial\xi}{\partial y}\right|_{y=1}=(-1)^{\bar{N}}\bar{N}\pi\sin(\bar{M}\pi x).\end{aligned} \tag{50}$$

where $\bar{M}, \bar{N}$ are angular velocity parameters.

In our approach, the boundary matrices are expressed by

$$h_{j,k}(x)=\varphi_{j,k}(x)|_{p_{0,1,i}\to 0,p_{1,1,i}\to 0},\quad h_{j,l}(y)=\varphi_{j,l}(y)|_{p_{0,1,i}\to 0,p_{1,1,i}\to 0.} \tag{51}$$

Therefore, $\xi(x, y)$ and $f(x, y)$ are approximated by

$$f(x,y)\approx P^j f(x,y)=\sum_{k=0}^{2^j}\sum_{l=0}^{2^j}f\left(\frac{k}{2^j},\frac{l}{2^j}\right)\varphi_{j,k}(x)\varphi_{j,l}(y), \tag{52}$$

$$\xi(x,y)\approx P^j\xi(x,y)=\sum_{k=0}^{2^j}\sum_{l=0}^{2^j}\xi\left(\frac{k}{2^j},\frac{l}{2^j}\right)h_{j,k}(x)h_{j,l}(y)+B'_{\xi}, \tag{53}$$

where

$$\begin{aligned}B'_{\xi}=&\bar{M}\pi\left\{\sum_{k=0}^{2^j}\sin\left(\frac{\bar{M}\pi k}{2^j}\right)h_{j,k}(x)\left[\varphi^0_{j,1}(y)+(-1)^{\bar{M}}\varphi^1_{j,1}(y)\right]\right\}\\ &+\bar{N}\pi\left\{\sum_{l=0}^{2^j}\sin\left(\frac{\bar{N}\pi l}{2^j}\right)h_{j,l}(y)\left[\varphi^0_{j,1}(x)+(-1)^{\bar{N}}\varphi^1_{j,1}(x)\right]\right\}.\end{aligned}$$

Multiplying $h_{j,n}(x)h_{j,m}(y)$ on both sides of the above equations, and applying the multiple integrals on interval $[0, 1]^2$, we obtain

$$\tilde{\mathbf{A}}_3\bullet\hat{\mathbf{U}}_3+\tilde{\mathbf{B}}_3\bullet\hat{\mathbf{F}}+\sum_{i=1}^{4}\tilde{\mathbf{C}}_i\bullet\hat{\mathbf{S}}_i=\mathbf{0}. \tag{54}$$

where the straight vectors of the variable $\xi(x, y)$ and $f(x, y)$ are written as

$$\hat{\mathbf{U}}_3=\left\{\xi_p=\xi\left(\frac{k}{2^j},\frac{l}{2^j}\right)\right\},\quad \hat{\mathbf{F}}=\left\{f_p=f\left(\frac{k}{2^j},\frac{l}{2^j}\right)\right\}.$$

and the boundary vectors are

$$\begin{aligned}&\hat{\mathbf{S}}_1=\left\{s^1_k=\bar{M}\pi\sin\left(\frac{\bar{M}\pi k}{2^j}\right)\right\},\quad \hat{\mathbf{S}}_2=\left\{s^2_k=(-1)^{\bar{M}}\bar{M}\pi\sin\left(\frac{\bar{M}\pi k}{2^j}\right)\right\},\\ &\hat{\mathbf{S}}_3=\left\{t^1_l=\bar{N}\pi\sin\left(\frac{\bar{N}\pi l}{2^j}\right)\right\},\quad \hat{\mathbf{S}}_4=\left\{t^2_l=(-1)^{\bar{N}}\bar{N}\pi\sin\left(\frac{\bar{N}\pi l}{2^j}\right)\right\}.\end{aligned} \tag{55}$$

The iterating matrix are

$$\begin{aligned}&\tilde{\mathbf{A}}^T_3=\mathbf{\Gamma}^{j,2}_{k,n}\bigotimes\mathbf{\Gamma}^{j,0}_{l,m}+\pi^2\mathbf{\Gamma}^{j,0}_{k,n}\bigotimes\mathbf{\Gamma}^{j,0}_{l,m}+\mathbf{\Gamma}^{j,0}_{k,n}\bigotimes\mathbf{\Gamma}^{j,2}_{l,m},\tilde{\mathbf{B}}^T_3=\bar{\mathbf{\Gamma}}^{j,0}_{k,n}\bigotimes\bar{\mathbf{\Gamma}}^{j,0}_{l,m},\\ &\tilde{\mathbf{C}}^T_1=\mathbf{\Gamma}^{j,2}_{k,n}\bigotimes\hat{\mathbf{\Gamma}}^{j,0}_{L,m}+\mathbf{\Gamma}^{j,0}_{k,n}\bigotimes\hat{\mathbf{\Gamma}}^{j,2}_{L,m},\tilde{\mathbf{C}}^T_2=\mathbf{\Gamma}^{j,2}_{k,n}\bigotimes\hat{\mathbf{\Gamma}}^{j,0}_{R,m}+\mathbf{\Gamma}^{j,0}_{k,n}\bigotimes\hat{\mathbf{\Gamma}}^{j,2}_{R,m},\\ &\tilde{\mathbf{C}}^T_3=\hat{\mathbf{\Gamma}}^{j,0}_{L,n}\bigotimes\mathbf{\Gamma}^{j,2}_{l,m}+\hat{\mathbf{\Gamma}}^{j,2}_{L,n}\bigotimes\mathbf{\Gamma}^{j,0}_{l,m},\tilde{\mathbf{C}}^T_4=\hat{\mathbf{\Gamma}}^{j,0}_{R,n}\bigotimes\mathbf{\Gamma}^{j,2}_{l,m}+\hat{\mathbf{\Gamma}}^{j,2}_{R,n}\bigotimes\mathbf{\Gamma}^{j,0}_{l,m},\\ &o=2^jn+m+1,\quad p=2^jk+l+1,\quad k,l,n,m=0\sim 2^j.\end{aligned}$$

Table 2
Approximation time and precision in 2D linear equations governed by Laplace and Biharmonic operators.

Operators	j	3	4	5	6
Laplace(∇^2)	$ErrSQ_\xi$	3.798E−03	5.050E−04	2.706E−05	5.558E−06
	CPU time(s)	2.525	3.901	7.359	57.842
Biharmonic(∇^4)	$ErrSQ_\xi$	6.349E−07	4.518E−09	1.636E−10	2.423E−12
	CPU time(s)	3.143	2.956	6.339	51.366

The other example is governed by the biharmonic operator with the function $f(x, y)$ being not zero on boundaries

$$\begin{aligned}&\frac{\partial^4\xi}{\partial x^4}+2\frac{\partial^4\xi}{\partial x^2\partial y^2}+\frac{\partial^4\xi}{\partial y^4}+\frac{\partial^2\xi}{\partial x\partial y}+f=0,\\&f=-(\bar{M}^4+2\bar{M}^2\bar{N}^2+\bar{N}^4)\pi^4\sin(\bar{M}\pi x)\sin(\bar{N}\pi y)\\&\quad-\pi^2\bar{M}\bar{N}\cos(\bar{M}\pi x)\cos(\bar{N}\pi y),\end{aligned}\tag{56}$$

subjected to the Cauchy type boundary conditions (50), together with the following add-in Dirichlet conditions.

$$\xi|_\Gamma=0,\quad \Gamma=[0,1]\times[0,1].\tag{57}$$

Note that this equation has the analytical solution given in Eq. (49).

The Coiflets modifications for $\xi(x, y)$ are exactly same as Eq. (51) but the approximations is different from Eq. (53)

$$\xi(x,y)\approx P^j\xi(x,y)=\sum_{k'=1}^{2^j-1}\sum_{l'=1}^{2^j-1}\xi\left(\frac{k'}{2^j},\frac{l'}{2^j}\right)h_{j,k'}(x)h_{j,l'}(y)+B'_\xi.\tag{58}$$

the source item $f(x, y)$ is same as Eq. (52) that can not simplified since it is not equal to zero at the boundaries. Multiplying $h_{j,n'}(x)h_{j,m'}(y)$ on both sides and then integrating with the help of the Wavelet–Galerkin method, we obtain

$$\tilde{\mathbf{A}}_4\bullet\hat{\mathbf{U}}_4+\tilde{\mathbf{B}}_4\bullet\hat{\mathbf{F}}+\sum_{i=1}^{4}\tilde{\mathbf{D}}_i\bullet\hat{\mathbf{S}}_i=\mathbf{0}.$$

where the straight vectors and systematic iterating matrixes are listed as

$$\hat{\mathbf{U}}_4=\left\{\xi_{p'}=\xi\left(\tfrac{k'}{2^j},\tfrac{l'}{2^j}\right)\right\},\quad \tilde{\mathbf{B}}_4^T=\bar{\mathbf{\Gamma}}_{k,n'}^{j,0}\otimes\bar{\mathbf{\Gamma}}_{l,m'}^{j,0},$$
$$\tilde{\mathbf{A}}_4^T=\mathbf{\Xi}_{4,0}+2\mathbf{\Xi}_{2,2}+\mathbf{\Xi}_{0,4},\quad \mathbf{\Xi}_{s,t}=\mathbf{\Gamma}_{k',n'}^{j,s}\otimes\mathbf{\Gamma}_{l',m'}^{j,t}.$$

The boundary vectors are identical to Eq. (55), while the tensors of the nonhomogeneous boundary conditions are

$$\tilde{\mathbf{D}}_i^T=\mathbf{\Xi}_{4,0}^i+2\mathbf{\Xi}_{2,2}^i+\mathbf{\Xi}_{0,4}^i+\mathbf{\Xi}_{1,1}^i,\quad i=1,2,3,4,\tag{59}$$

where iterating matrices and suffix are

$$\begin{aligned}&\mathbf{\Xi}_{s,t}^1=\mathbf{\Gamma}_{k,n'}^{j,s}\bigotimes\hat{\mathbf{\Gamma}}_{L,m'}^{j,t},\quad \mathbf{\Xi}_{s,t}^2=\mathbf{\Gamma}_{k,n'}^{j,s}\bigotimes\hat{\mathbf{\Gamma}}_{R,m'}^{j,t},\\&\mathbf{\Xi}_{s,t}^3=\hat{\mathbf{\Gamma}}_{L,n'}^{j,s}\bigotimes\mathbf{\Gamma}_{l,m'}^{j,t},\quad \mathbf{\Xi}_{s,t}^4=\hat{\mathbf{\Gamma}}_{R,n'}^{j,s}\bigotimes\mathbf{\Gamma}_{l,m'}^{j,t},\\&o'=(2^j-1)(n'-1)+m',\quad p'=(2^j-1)(k'-1)+l',\\&p=2^jk+l+1,\quad k,l=0\sim2^j,\quad k',n',l',m'=1\sim2^j-1.\end{aligned}$$

For the Laplace equation with Neumann boundary conditions and the Biharmonic equation with Cauchy boundary conditions, we select the iterating dimensions are $(2^j+1)\times(2^j+1)$ and $(2^j-1)\times(2^j-1)$ respectively to make equations closed. As shown in Table 2, for both cases, the average square errors decrease with the resolution level j increasing. For $j=6$ and the approaching items numbers are 64×64, the errors reach to 10^{-6} and 10^{-12} respectively in less than 1 min. Also, it can be seen from Fig. 3, our results match the analytical ones. This shows very good computational efficiency of our proposed technique.

4. Homotopy-wavelet approach for steady flow in a lid-driven cavity

It has been known that our proposed technique is valid for linear problems with nonhomogeneous boundary conditions. Here we examine its potentials for nonlinear problems. The classical problem of 2-D incompressible steady flow in a lid-driven cavity with two singular points of velocity field on rigid is a typical example to testify the validity and efficiency of our approach. The overall calculations are conducted in a desktop computer(CPU Intel Core TM i5-4460 CPU @3.20 GHz, Memory 8 GB).

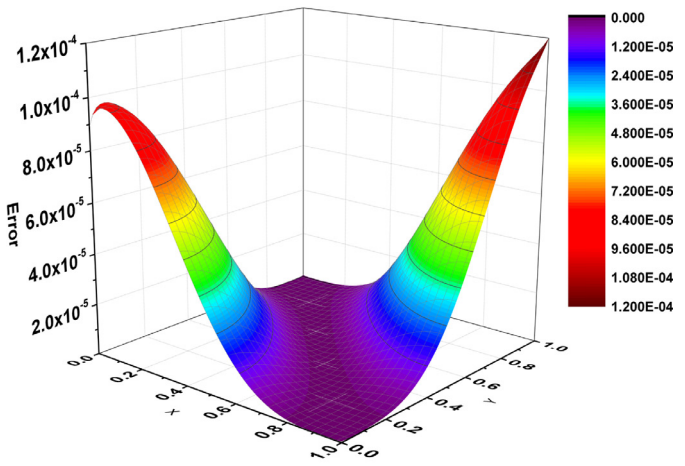

(a) Laplace 2-D case ($j = 5$).

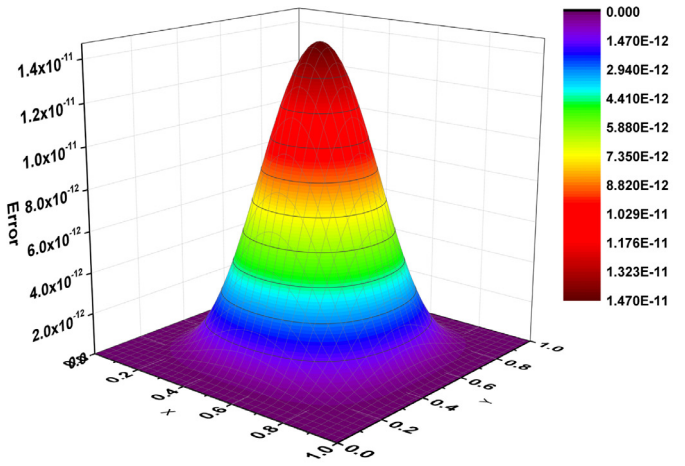

(b) Biharmonic 2-D case ($j = 6$)

Fig. 3. Solution error distributions of linear 2-D equations governed by Laplace operator subjected to Neumann boundary and Biharmonic operator subjected to Cauchy boundary.

Many researchers have studied various aspects of the cavity flow problems by different numerical methods in different Reynolds and formulation, as showed in Table 3. The governing equations of 2D lid driven cavity flow are usually two forms. One is the stream function-vorticity formulation with eliminating the pressure field by introducing stream function to simplify the original equations. Another is the form of original coupled equations for velocity and pressure field.

The cavity flow problem is demonstrated as a benchmark to validate efficiency of various algorithms, such as the Finite Difference Method(FDM) [23–25], the Finite Element Method(FEM) [26,27], the Finite Volume Method(FVM) [28], the Lattice Boltzmann Method(LBM) [29], the Boundary Element Method(BEM)[30,31], the Wavelet BEM-FEM [32–34], the Spectral Method [35] with different range of Reynolds and grid discretization [36]. The benchmark data were elaborated by Ghia et al. [37], Botella and Peyret [38], Bruneau and Saad [39], and Marchi et al. [40], respectively. Due to the strong nonlinearity of the governing equation and its nonhomogeneous boundaries, analytic solutions to this problems is extremely difficult to give by analytical approaches.

As shown in Fig. 4, the classic 2-D incompressible viscous cavity flow is governed by $\psi - \omega$ equation in the following form

$$\nabla^2\omega = \frac{\partial^2\omega}{\partial x^2} + \frac{\partial^2\omega}{\partial y^2} = Re\left(\frac{\partial\omega}{\partial x}\frac{\partial\psi}{\partial y} - \frac{\partial\omega}{\partial y}\frac{\partial\psi}{\partial x}\right),$$

$$\nabla^2\psi = \frac{\partial^2\psi}{\partial x^2} + \frac{\partial^2\psi}{\partial y^2} = -\omega,$$

Table 3
References with governing equations formulation and grid scale for the classical cavity driven flow.

Authors	*Formulation*	*Re*	*Methods*	*Grids*
Kawaguiti [42]	$\psi-\omega$	$0-64$	FDM	11×11
Burggraf [43]	$\psi-\omega$	$0-700$	FDM	$11\times 11\sim 51\times 51$
Rubin and Khosla [23]	$\psi-\omega$	100 &1000	FDM	$17\times 17\sim 128\times 128$
Benjamin and Denny [24]	$\psi-\omega$	$1000\sim 10000$	FDM	$61\times 61\sim 151\times 151$
Ghia et al. [37]	$\psi-\omega$	$100\sim 10000$	FDM	$129\times 129\sim 257\times 257$
Schreiber and Keller [44]	$\psi-\omega$	$1\sim 10000$	FDM	$121\times 121\sim 180\times 180$
Vanka [45]	u, v, p	$100\sim 5000$	FDM	$41\sim 41\sim 321\sim 321$
Nishida and Satofuka [46]	$\psi-\omega$	$100\sim 3200$	FDM	$65\times 65\sim 129\times 129$
Liao [30]	$\psi-\omega$	$100\sim 2000$	BEM	64×64
Hou et al. [29]	LBE	$100\sim 7500$	LBM	256×256
Wright and Gaskell [47]	u, v, p	100&1000	FVM	1024×1024
Goyon [48]		1000	FDM	129×129
Barragy and Carey [49]	$\psi-\omega$	$0.0001\sim 10000$	FEM	257×257
Botella and Peyret [38]	u, v, p	100 & 1000	Spectral	160
Zhang [50]	$\psi-\omega$	$100\sim 7500$	FDM	$17\times 17\sim 129\times 129$
Zhao and Liao [31]	$\psi-\omega$	$1000\sim 10000$	BEM	64×64
Ravnik et al. [32]		400	Wavelet BEM-FEM	120eqs
Gupta et al. [51]	$\psi-V$	$100\sim 10000$	FDM	$41\times 41\sim 161\times 161$
Erturk et al. [52]	$\psi-\omega$	$100\sim 21000$	FDM	401×401
Bruneau and Saad [39]	u, v, p	$1000\sim 10000$	FDM	$128\times 128\sim 2048\times 2048$
Marchi et al. [40]	u, v, p	$0.01\sim 1000$	FVM	$2\times 2\sim 1024\times 1024$
This work	$\psi-\omega$	$0.01\sim 2000$	wHAM	$8\times 8(j=3)\sim 64\times 64(j=6)$

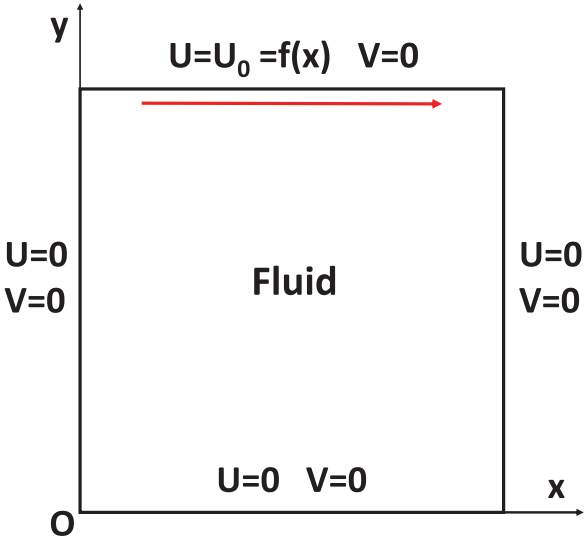

Fig. 4. Schematic diagram and boundary conditions of viscous flow in a Cavity.

$$\bar{u}=\frac{\partial\psi}{\partial y}\quad \bar{v}=-\frac{\partial\psi}{\partial x}. \tag{60}$$

subjected to the no-slip and impenetrable boundary conditions

$$\begin{aligned}
&\bar{u}=\frac{\partial\psi}{\partial y}=0,\quad \bar{v}=-\frac{\partial\psi}{\partial x}=0,\quad \text{on}\quad x=0,\\
&\bar{u}=\frac{\partial\psi}{\partial y}=0,\quad \bar{v}=-\frac{\partial\psi}{\partial x}=0,\quad \text{on}\quad x=1,\\
&\bar{u}=\frac{\partial\psi}{\partial y}=0,\quad \bar{v}=-\frac{\partial\psi}{\partial x}=0,\quad \text{on}\quad y=0,\\
&\bar{u}=\frac{\partial\psi}{\partial y}=f(x),\quad \bar{v}=-\frac{\partial\psi}{\partial x}=0,\quad \text{on}\quad y=1.
\end{aligned} \tag{61}$$

where ψ is the stream function, ω is the vortex function, $\bar{u}, \bar{v}$ are velocities in x, y direction, respectively. It should be noted here that the closed wavelet method does not work for this problem since the boundary conditions are unable to be transformed into homogeneous ones.

4.1. Mathematical formulation

As illustrated above, our approach works well for differential equations with the mixed Cauchy boundary conditions. Hence we make attempt to convert the boundary conditions (61) for ψ to Cauchy ones.

Due to the border speciality of the rectangular computational domain, ψ is single-valued function of x when y is prescribed, or vice versa. Choosing an arbitrary point $P = (0, y_P)$ and its neighboring point $P_1 = (0, y_P + \delta)$, employing the single-valued function $\hat{\psi}(y)$ at $x = 0$, the derivative of $\psi(x, y)$ can expressed by

$$\left.\frac{\partial \psi(x,y)}{\partial y}\right|_{x=0} = \frac{\psi_{p_1} - \psi_p}{\overrightarrow{PP_1}} = \frac{\hat{\psi}_{p_1}(y+\delta) - \hat{\psi}_p(y)}{\delta} = 0.$$

Since δ is an arbitrary small amount and P is a random point, we are able to assume $\psi = C_1$ at $x = 0$. Similarly, taking account of the no-slip boundary conditions on other three sides, $\psi \in C^4[0, 1]$ is constant for four boundary edges. It is known that the velocity field is only determined by the derivatives of ψ, so we can prescribe this constant without changing behaviours for the original problems. For simplicity, we set $\psi = 0$ on the boundaries such that the mixed nonhomogeneous Cauchy boundary conditions are

$$\begin{aligned} &x = 0, \quad \psi = 0, \quad \frac{\partial \psi}{\partial x} = 0; \quad x = 1, \quad \psi = 0, \quad \frac{\partial \psi}{\partial x} = 0; \\ &y = 0, \quad \psi = 0, \quad \frac{\partial \psi}{\partial y} = 0; \quad y = 1, \quad \psi = 0, \quad \frac{\partial \psi}{\partial y} = f(x). \end{aligned} \tag{62}$$

By eliminating the vortex ω and adding the source item Q, Eq. (60) is reduced to

$$\nabla^2\nabla^2\psi + Re\left(\frac{\partial \psi}{\partial x}\frac{\partial^3 \psi}{\partial y^3} + \frac{\partial \psi}{\partial x}\frac{\partial^3 \psi}{\partial x^2 \partial y} - \frac{\partial \psi}{\partial y}\frac{\partial^3 \psi}{\partial x^3} - \frac{\partial \psi}{\partial y}\frac{\partial^3 \psi}{\partial x \partial y^2}\right) = Q. \tag{63}$$

Here Q is used to validate convergence and it equates to 0 in later computation.

4.2. Solutions by the HAM with the generalized orthogonal Coiflets

We combine the HAM technique with Coiflets to give the exact wavelet approximations to this cavity problem. We first transform the nonlinear equation into a set of linear homogenous ones. In the framework of the HAM technique, the zeroth-order deformation equation is constructed as

$$(1 - p)\mathcal{L}_\psi[\Phi(x, y; p) - \psi_0(x, y)] = pc_0\mathcal{N}_\psi[\Phi(x, y; p)]. \tag{64}$$

where p is the embedding parameter, c_0 is the convergence-control parameter, $\mathcal{L}$ is the linear operator given by

$$\mathcal{L}_\psi[f] = \nabla^4[f] = \frac{\partial^4}{\partial x^4} + 2\frac{\partial^4}{\partial x^2 \partial y^2} + \frac{\partial^4}{\partial y^4}[f], \tag{65}$$

and $\mathcal{N}_\psi[\Phi]$ is the nonlinear operator defined by

$$\mathcal{N}_\psi[\Phi] = \nabla^4\Phi + Re\left(\frac{\partial \Phi}{\partial x}\frac{\partial^3 \Phi}{\partial y^3} + \frac{\partial \Phi}{\partial x}\frac{\partial^3 \Phi}{\partial x^2 \partial y} - \frac{\partial \Phi}{\partial y}\frac{\partial^3 \Phi}{\partial x^3} - \frac{\partial \Phi}{\partial y}\frac{\partial^3 \Phi}{\partial x \partial y^2}\right) - Q. \tag{66}$$

Note that for $p = 0$ and $p = 1$, we have respectively

$$\Phi(x, y; 0) = \psi_0(x, y), \quad \Phi(x, y; 1) = \psi(x, y). \tag{67}$$

As p increases from 0 to 1, $\Phi(x, y; p)$ varies from the initial guess $\psi_0(x, y)$ to the desired solution $\psi(x, y)$. Using the Taylor expansion, $\Phi(x, y; p)$ can be expanded with respect to p in the following form

$$\Phi(x, y; p) = \psi_0(x, y) + \sum_{M=1}^{+\infty} \psi_M(x, y)p^m, \tag{68}$$

where

$$\psi_M(x,y)=\frac{1}{M!}\frac{\partial^M\Phi(x,y;p)}{\partial p^M}\bigg|_{p=0}. \tag{69}$$

If the auxiliary linear operator, the initial guess, and the convergence-control parameter are chosen properly so the Taylor series all converge at $p=1$, we obtain the homotopy-series solutions

$$\psi(x,y)=\psi_0(x,y)+\sum_{M=1}^{+\infty}\psi_M(x,y). \tag{70}$$

The Mth-order deformation equation can be obtained, by differentiating Eq. (64) with respect to p for M times, and then setting $p=0$, as

$$\mathcal{L}_\psi[\psi_M-\chi_M\psi_{M-1}]=c_0\left\{\nabla^4\psi_{M-1}+R_M+(\chi_M-1)Q\right\} \tag{71}$$

where

$$R_M=Re\sum_{s=0}^{M-1}\left\{\frac{\partial\psi_s}{\partial x}\frac{\partial^3\psi_{M-1-s}}{\partial y^3}+\frac{\partial\psi_s}{\partial x}\frac{\partial^3\psi_{M-1-s}}{\partial x^2\partial y}-\left(\frac{\partial\psi_s}{\partial y}\frac{\partial^3\psi_{M-1-s}}{\partial x^3}+\frac{\partial\psi_s}{\partial y}\frac{\partial^3\psi_{M-1-s}}{\partial x\partial y^2}\right)\right\}$$

and

$$\chi_{\bar{k}}=\begin{cases}0, & \bar{k}\le 1,\\ 1, & \bar{k}>1.\end{cases} \tag{72}$$

The Coiflets used for the nonhomogeneous boundary conditions are taken into consideration by setting

$$h_{j,k}(x)=\varphi_{j,k}(x)|_{p_{0,1,i}\to 0,\,p_{1,1,i}\to 0}\quad h_{j,l}(y)=\varphi_{j,l}(y)|_{p_{0,1,i}\to 0,\,p_{1,1,i}\to 0}$$
$$\varpi_{j,L}(x)=0,\quad \varpi_{j,R}(x)=\varpi^1_{j,1}(x).$$

Therefore, the wavelet approximations for each order stream function $\psi_M(x,y)$ and its derivatives are written, at $u=v=0$, as

$$\frac{\partial^{u+v}\psi_M}{\partial x^u\partial y^v}\approx\sum_{k'=1}^{2^j-1}\sum_{l'=1}^{2^j-1}\psi_M\left(\frac{k'}{2^j},\frac{l'}{2^j}\right)h^{(u)}_{j,k'}(x)h^{(v)}_{j,l'}(y)+(1-\chi_{M+1})\sum_{k=0}^{2^j}f\left(\frac{k}{2^j}\right)h^{(u)}_{j,k}(x)\varpi^{(v)}_{j,R}(y). \tag{73}$$

In our analysis, the coefficients of wavelet series are given at level j, while the reconstitution for the stream function, the vortex and the velocity are showed at level J. Note that J is reconstitution level and j is resolution level, respectively. In generalized orthogonal Coiflets system, we set $J=j$ for simplicity and more detailed is illustrated in Appendix A. In this way, we reconstitute

$$\psi(x,y)\approx S^j\psi(x,y)=\sum_{k'=1}^{2^j-1}\sum_{l'=1}^{2^j-1}\psi\left(\frac{k'}{2^j},\frac{l'}{2^j}\right)h_{j,k'}(x)h_{j,l'}(y)+\sum_{k=0}^{2^j}f\left(\frac{k}{2^j}\right)h_{j,k}(x)\varpi_{j,R}(y), \tag{74}$$

$$\begin{aligned}\omega(x,y)\approx -S^j\Delta\psi(x,y)=&-\sum_{k'=1}^{2^j-1}\sum_{l'=1}^{2^j-1}\psi\left(\frac{k'}{2^j},\frac{l'}{2^j}\right)\left[h^{(2)}_{j,k'}(x)h_{j,l'}(y)\right.\\&\left.+h_{j,k'}(x)h^{(2)}_{j,l'}(y)\right]-\sum_{k=0}^{2^j}f\left(\frac{k}{2^j}\right)\left[h^{(2)}_{j,k}(x)\varpi_{j,R}(y)+h_{j,k}(x)\varpi^{(2)}_{j,R}(y)\right],\end{aligned} \tag{75}$$

$$\bar{u}(x,y)\approx\sum_{k'=1}^{2^j-1}\sum_{l'=1}^{2^j-1}\psi\left(\frac{k'}{2^j},\frac{l'}{2^j}\right)h_{j,k'}(x)h^{(1)}_{j,l'}(y)+\sum_{k=0}^{2^j}f\left(\frac{k}{2^j}\right)h_{j,k}(x)\varpi^{(1)}_{j,R}(y), \tag{76}$$

$$\bar{v}(x,y)\approx-\sum_{k'=1}^{2^j-1}\sum_{l'=1}^{2^j-1}\psi\left(\frac{k'}{2^j},\frac{l'}{2^j}\right)h^{(1)}_{j,k'}(x)h_{j,l'}(y)-\sum_{k=0}^{2^j}f\left(\frac{k}{2^j}\right)h^{(1)}_{j,k}(x)\varpi_{j,R}(y). \tag{77}$$

Substituting Eq. (73) into Eq. (71), we can approximate the solutions for ψ, at Mth order HAM deformation equations, as

$$\begin{aligned}&\sum_{k'=1}^{2^j-1}\sum_{l'=1}^{2^j-1}\left\{\psi_M\left(\frac{k'}{2^j},\frac{l'}{2^j}\right)\mathcal{L}_\psi[h_{j,k'}(x)h_{j,l'}(y)]\right.\\&\left.-\psi_{M-1}\left(\frac{k'}{2^j},\frac{l'}{2^j}\right)\left\{\chi_M\mathcal{L}_\psi[h_{j,k'}(x)h_{j,l'}(y)]+c_0\nabla^4[h_{j,k'}(x)h_{j,l'}(y)]\right\}\right\}\\&=c_0(1-\chi_M)\sum_{k=0}^{2^j}f\left(\frac{k}{2^j}\right)\nabla^4[h_{j,k}(x)\varphi_{j,R}(y)]\end{aligned}$$

$$-c_0\sum_{k=0}^{2^j}\sum_{l=0}^{2^j}\left[R_M\left(\frac{k}{2^j},\frac{l}{2^j}\right)+(1-\chi_M)Q\left(\frac{k}{2^j},\frac{l}{2^j}\right)\right]\varphi_{j,k}(x)\varphi_{j,l}(y). \tag{78}$$

Multiplying $h_{j,n'}(x)h_{j,m'}(y)$ on both sides of Eq. (78) and integrating on the domain $[0, 1]^2$, we obtain the iterative equation

$$\hat{\mathbf{\Psi}}_M^s=(c_0+\chi_M)\hat{\mathbf{\Psi}}_{M-1}^s+c_0\tilde{\mathbf{A}}_\psi^{-1}\bullet\tilde{\mathbf{R}}_M+c_0(1-\chi_M)\tilde{\mathbf{A}}_\psi^{-1}\bullet(\tilde{\mathbf{P}}_B-\tilde{\mathbf{P}}_Q). \tag{79}$$

where the straight vectors and the systematic iterative tensors are given by

$$\begin{aligned}
\hat{\mathbf{\Psi}}_M^s&=\left\{\psi_{p'}=\psi_M\left(\frac{k'}{2^j},\frac{l'}{2^j}\right)\right\}\\
\tilde{\mathbf{A}}_\psi^T&=\mathbf{\Gamma}_{k',n'}^{j,4}\bigotimes\mathbf{\Gamma}_{l',m'}^{j,0}+2\mathbf{\Gamma}_{k',n'}^{j,2}\bigotimes\mathbf{\Gamma}_{l',m'}^{j,2}+\mathbf{\Gamma}_{k',n'}^{j,0}\bigotimes\mathbf{\Gamma}_{l',m'}^{j,4},\\
p'&=(2^j-1)(k'-1)+l',\quad k',l',n',m'=1\sim 2^j-1.
\end{aligned}$$

Iterative correction tensor $\tilde{\mathbf{P}}_B$ resulting from nonhomogeneous boundaries are written as

$$\begin{aligned}
&\tilde{\mathbf{P}}_B=\tilde{\mathbf{T}}_R\bullet\hat{\mathbf{S}}_R,\quad \hat{\mathbf{S}}_R=\left\{s_k^r=f\left(\frac{k}{2^j}\right)\right\},\\
&\tilde{\mathbf{T}}_R^T=\mathbf{\Gamma}_{k,n'}^{j,4}\bigotimes\hat{\mathbf{\Gamma}}_{R,m'}^{j,0}+2\mathbf{\Gamma}_{k,n'}^{j,2}\bigotimes\hat{\mathbf{\Gamma}}_{R,m'}^{j,2}+\mathbf{\Gamma}_{k,n'}^{j,0}\bigotimes\hat{\mathbf{\Gamma}}_{R,m'}^{j,4}.
\end{aligned}$$

The straight vector of external item $\hat{\mathbf{Q}}$ and iterating matrix are expressed by

$$\hat{\mathbf{P}}_Q=\tilde{\mathbf{C}}_\psi\bullet\hat{\mathbf{Q}},\quad \hat{\mathbf{Q}}=\left\{q_p=Q\left(\frac{k}{2^j},\frac{l}{2^j}\right)\right\},\quad \tilde{\mathbf{C}}_\psi^T=\bar{\mathbf{\Gamma}}_{k,n'}^{j,0}\bigotimes\bar{\mathbf{\Gamma}}_{l,m'}^{j,0}.$$

It is worth mentioning that nonhomogeneous boundary affects the wavelet approaching precision for ψ_0, via Eqs. (A.8) and (A.9), we therefore write

$$\hat{\mathbf{\Psi}}_{u,v}^{M,j}=\left(\widetilde{\mathbf{\Phi}}_u^j\bigotimes\widetilde{\mathbf{\Phi}}_v^j\right)^T\bullet\hat{\mathbf{\Psi}}_M^U+(1-\chi_{M+1})\left(\widetilde{\mathbf{\Phi}}_v^j\right)^T\bullet\left(\tilde{\mathbf{S}}_R\bigotimes\widetilde{\mathbf{\Phi}}_{u,R}^j\right). \tag{80}$$

where the straight vectors of point value and the tensors are

$$\begin{aligned}
&\hat{\mathbf{\Psi}}_M^U=\left\{\psi_o=\psi_M\left(\frac{k}{2^j},\frac{l}{2^j}\right)\right\},\quad \widetilde{\mathbf{\Phi}}_{u,R}^j=\left\{b_{j,s}=\varpi_{j,R}^{(u)}\left(\frac{s}{2^j}\right)\right\}.\\
&\hat{\mathbf{\Psi}}_{u,v}^{M,j}=\left\{\psi_p^j=\frac{\partial^{u+v}\psi}{\partial x^u\partial y^v}\left(\frac{s}{2^j},\frac{t}{2^j}\right)\right\},\\
&o=2^jk+l+1,\quad p=2^js+t+1,\quad k,l,s,t=0\sim 2^j.
\end{aligned}$$

The straight vector of nonlinear part is regarded as a single function approximated by former Coiflets is

$$\tilde{\mathbf{R}}_M=\tilde{\mathbf{C}}_\psi\bullet\hat{\mathbf{R}}_M,\quad \hat{\mathbf{R}}_M=\left\{r_p=R_M\left(\frac{k}{2^j},\frac{l}{2^j}\right)\right\}.$$

Finally, Mth nonlinear part are approximated by each ψ_M as

$$\hat{\mathbf{R}}_M=Re\sum_{s=0}^{M-1}\left[\hat{\mathbf{\Psi}}_{1,0}^{s,j}\bigodot\hat{\mathbf{\Psi}}_{0,3}^{M-1-s,j}+\hat{\mathbf{\Psi}}_{1,0}^{s,j}\bigodot\hat{\mathbf{\Psi}}_{2,1}^{M-1-s,j}-\hat{\mathbf{\Psi}}_{0,1}^{s,j}\bigodot\hat{\mathbf{\Psi}}_{3,0}^{M-1-s,j}-\hat{\mathbf{\Psi}}_{0,1}^{s,j}\bigodot\hat{\mathbf{\Psi}}_{1,2}^{M-1-s,j}\right].$$

Because of the strong nonlinearity of the nonlinear part R_M, it is very time-consuming with the computational order M increasing. To overcome this deficiency, we apply homotopy iteration by transforming Mth results into the renew initial guess to accelerate the convergence, that is to say

$$\psi_{iter}=\psi_{initial}+\sum_{i=1}^{M}\psi_i(x,y)\to\psi_{initial}. \tag{81}$$

The computational errors are given, similar to Eqs. (46) and (47), as

$$ErrSQ_f = ||Err_f||_{\mathbf{L}^2[0,1]} \approx \frac{1}{(2^j+1)^2}\sum_{k=0}^{2^j}\sum_{l=0}^{2^j}\left[f\left(\frac{k}{2^j},\frac{l}{2^j}\right) - f_e\left(\frac{k}{2^j},\frac{l}{2^j}\right)\right]^2. \tag{82}$$

where $f = \psi, \omega, \bar{u}, \bar{v}, \bar{V}$ are the wavelet approximations and $f_e = \psi_e, \omega_e, \bar{u}_e, \bar{v}_e, \bar{V}_e$ are the analytical ones.

4.3. Convergence check and error analysis

To compare the validity and correctness of our wavelet approximations, we constitute a particular equation that contains an analytical solution. In this case, the external term Q is chosen as

$$\begin{aligned} Q(x,y) = {} & 128[-1+3y-3y^2+3y^3+112Re\cdot x^6y(1-3y+3y^2) \\ & -32Re\cdot x^7y(1-3y+3y^2)+48Re\cdot x^5y(-3+9y-7y^2-5y^3+3y^4) \\ & -40Re\cdot x^4y(-2+6y-15y^3+9y^4) \\ & +16Re\cdot x^3y(-1+3y+11y^2-35y^3+21y^4) \\ & +2x(-3+9y+8Re\cdot y^3-20Re\cdot y^4+12Re\cdot y^5) \\ & -6x^2(-1+3y+16Re\cdot y^3-40Re\cdot y^4+24Re\cdot y^5)]. \end{aligned} \tag{83}$$

So that we obtain the analytical expression for the stream function, the vortex, the velocity and its amplitude $\bar{V}$ as

$$\psi_e = 16x^2(1-x)^2y^2(y-1), \tag{84}$$

$$\omega_e = -32(6x^2-6x+1)(y-1)y^2 - 32(x-1)^2x^2(3y-1), \tag{85}$$

$$\bar{u}_e = 16(x-1)^2x^2y(3y-2), \tag{86}$$

$$\bar{v}_e = -32(x-1)x(2x-1)(y-1)y^2, \tag{87}$$

$$\bar{V}_e = 16\sqrt{(x-1)^2x^2y^2\left[(x-1)^2x^2(2-3y)^2+4(1-2x)^2(y-1)^2y^2\right]}. \tag{88}$$

Note that it corresponds to the velocity distribution on the upper plate

$$\bar{U}_0 = f(x) = 16x^2(1-x)^2. \tag{89}$$

We notice that the velocity $\bar{U}_0$ is equal to zero at $x = 0$ and $x = 1$. Therefore, the velocity distribution on the boundaries is continuous without singularity. As a result, Eq. (74) is simplified as

$$\psi(x,y) \approx \sum_{k'=1}^{2^j-1}\sum_{l'=1}^{2^j-1}\psi\left(\frac{k'}{2^j},\frac{l'}{2^j}\right)h_{j,k'}(x)h_{j,l'}(y) + \sum_{k'=1}^{2^j-1}f\left(\frac{k'}{2^j}\right)h_{j,k'}(x)\varpi_{j,R}(y). \tag{90}$$

To check the results, we define the error function $ErrRes_{\psi_M}$ as an indicator for convergence. Note that it is not sufficient to ensure the wavelet solutions converge to the analytical solutions. While it works well for the case that no analytical solution exists. The error function $ErrRes_{\psi_M}$ is defined as

$$ErrRes_{\psi_M} = ||\psi_M(x,y)||_{\mathbf{L}^2[0,1]} \approx \frac{1}{(2^j+1)^2}\sum_{k=0}^{2^j}\sum_{l=0}^{2^j}\psi_M\left(\frac{k}{2^j},\frac{l}{2^j}\right)^2. \tag{91}$$

Besides, $ErrX0.5(f, y)$ and $ErrX0.5(f, y)$ are defined as the error distributions of arbitrary 2D function $f(x, y)$ at $x = 0.5$ and $y = 0.5$

$$ErrX0.5(f,y) = \left|f(1/2,y) - f_e(y)\right|^2, \tag{92}$$

$$ErrY0.5(f,x) = \left|f(x,1/2) - f_e(x)\right|^2. \tag{93}$$

where $f_e(y)$ and $f_e(x)$ are the analytical solutions, respectively.

For a prescribed Reynolds number, our results agree well with the analytical ones, which shows great efficiency of our approach, as illustrated below. We first give the solution for $Re = 100$. As shown in Fig. 5, *ErrRes* decreases monotonously as the iterating time increases for all selected j. The CPU time of iteration reveals different scale of nearly $10^{j-3}(s)$ at different resolution level. Similarly, *ErrSQ* reduces rapidly to a certain scale as the iteration time enlarges. While as the iteration time is sufficiently large, it has limited effect on the improvement of solution accuracies. Note that we employee the homotopy iteration technique and the convergence control parameter is chosen as $-13/100$. More details on error computation are showed in Fig. 6. It is found that our wavelet results agree well with the analytical ones for $x = 0.5$ and

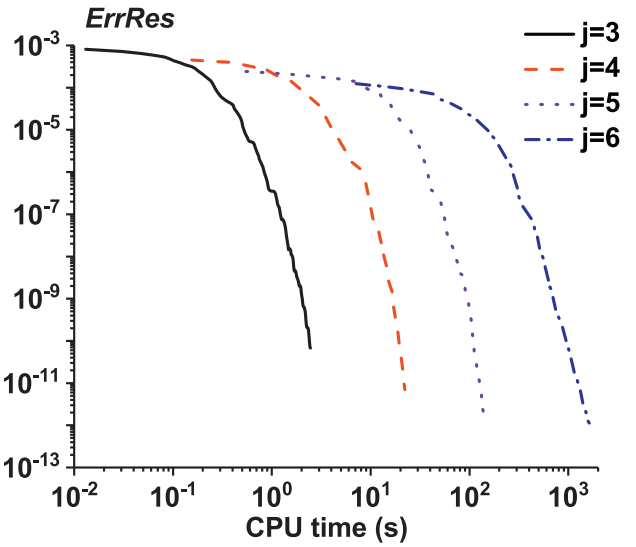

(a) $ErrRes$ of ψ when $j = 3 \sim 6$.

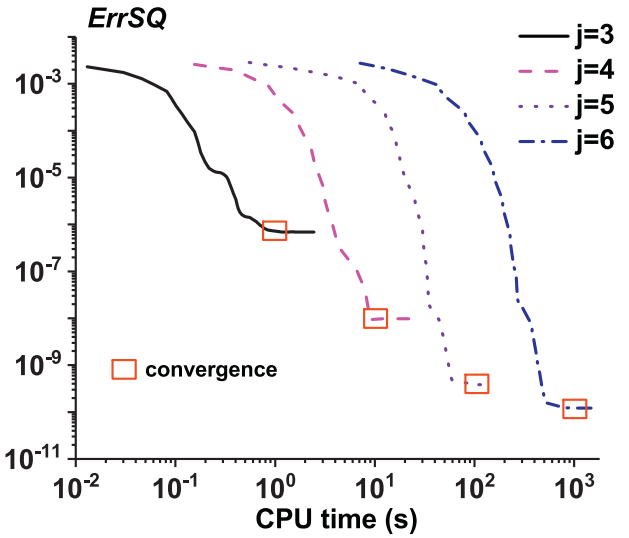

(b) $ErrSQ$ of ψ when $j = 3 \sim 6$.

Fig. 5. *ErrRes* and *ErrSQ* of ψ in different wavelet resolution levels vary with iterations when $Re = 100$.

$y = 0.5$, the maximum error ranges from 10^{-6} to 10^{-11}. In Fig. 7, it is found that the error distributions are very sensitive to the resolution level j, the larger is j, the error distribution contour is clearer.

Residuals for the fields of stream, the vortex and the velocity obtained also reveal good accuracies of our solutions. As showed in Table 4, by improving on the reconstitution level, from $j = 3$ to 5, the errors *ErrSQ* for $\psi, \omega, \bar{u}, \bar{v}, \bar{V}$ decrease at the rate of 10^{-2}. But regarding results of level $j = 6$, the iterating matrix $\tilde{\mathbf{A}}_{\psi}$ in the iterating Eq. (79) formed by connection coefficients is stiff without symmetry and is hard to be decomposed by *LU* technique with its dimension equaling 2^{2j} in 2D case. The improvement of j leads to the dramatic increase of the dimension with its inverse matrix difficult to be obtained with numerical errors and precision losses, which the accuracies are not improved obviously. Due to this reason, in the subsequent computation, we choose $j = 5$ for various Reynolds numbers.

As is known from Eqs. (75), (76) and (77), the reconstructions of $\bar{u}, \bar{v}, \bar{V}$ are associated with the first order derivatives of Coiflets, while ω is related to the second one. Based on the **Lemma** denoted in Eqs. (A.6) and (A.7), it is seen in Table 4 that the precision loss exists, this leads to that the accuracies for ψ is around $10^{-7}, 10^{-9}, 10^{-10}$, these for $\bar{u}, \bar{v}, \bar{V}$ are around $10^{-5}, 10^{-7}, 10^{-9}$, these for ω are $10^{-2}, 10^{-4}, 10^{-5}$ at $j = 3, 4, 5$, respectively.

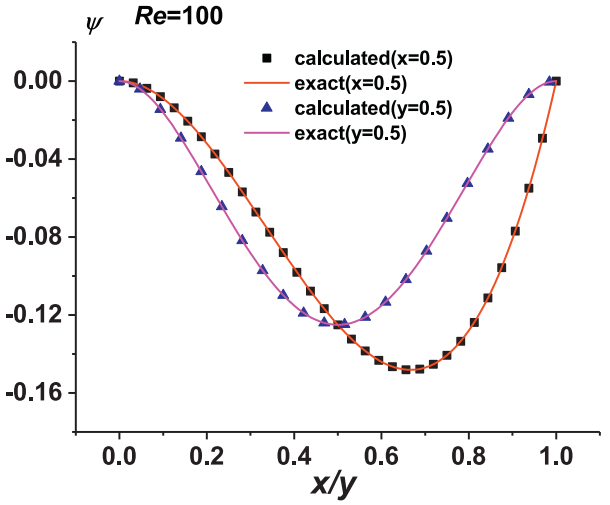

(a) Comparison at $x = 0.5$ and $y = 0.5$ when $j = 6$.

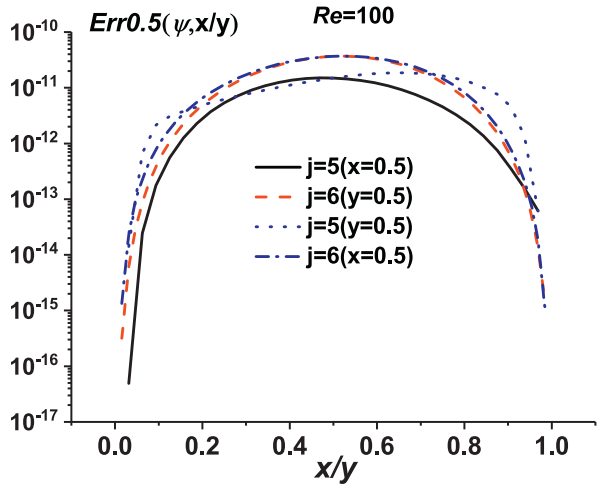

(b) Error distribution of ψ at $x = 0.5$ and $y = 0.5$.

Fig. 6. Comparison and error distributions of ψ on middle line at $x, y = 0.5$ in different wavelet resolution levels ($Re = 100$).

Table 4
Residues of $\psi, \omega, \bar{u}, \bar{v}, \bar{V}$ with different wavelet resolution levels by our approach with $M = 5$ and $iter = 30$ when $Re = 100$.

j	3	4	5	6
$ErrSQ_{\psi}$	6.845E−07	9.444E−09	1.237E−10	3.856E−11
$ErrSQ_{\omega}$	2.334E−02	8.172E−04	2.934E−05	1.303E−06
$ErrSQ_{\bar{u}}$	1.156E−05	1.189E−07	1.409E−09	4.796E−10
$ErrSQ_{\bar{v}}$	2.171E−05	2.510E−07	2.580E−09	4.435E−10
$ErrSQ_{\bar{V}}$	1.999E−05	2.550E−07	3.024E−09	7.142E−10
CPU time(s)	2.973	12.793	93.966	1578.016

As discussed above, our proposed approach can give exact approximations by selecting appropriate convergence control parameters. We use this property to compute the solutions for larger Reynolds number Re. The computational results for $Re = 200 \sim 500$ with $j = 5$ are showed Table 5. The convergence criterion is that the residuals $ErrSQ$ decrease continuously with increasing of the computational order. And at a certain order, the errors are less than the specified values in advance. Mathematically, the nonlinearity becomes stronger and stronger when Re grows gradually. To get highly accurate solutions, we must adjust the values of the convergence-control parameter c_0 and increase the computational order M. For these

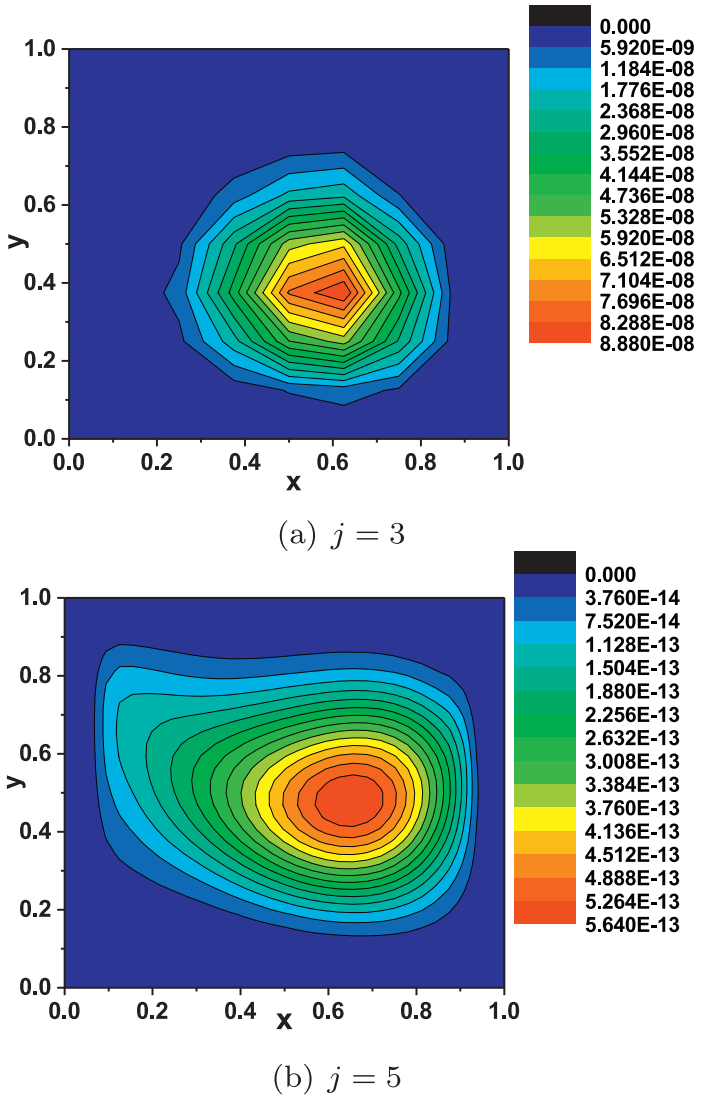

Fig. 7. Error distributions of ψ in different wavelet reconstitution levels when $j = 3, 5$.

Table 5
Residuals *ErrSQ* of $\psi, \omega, \bar{u}, \bar{v}, \bar{V}$,Time and c_0 when $Re = 100 \sim 500$ and $j = 5$.

Re	100	200	300	400	500
c_0	−0.13	−0.11	−0.05	−0.03	−0.02
$M \times iter$	108	254	750	1000	1500
$ErrRes_{\psi_M}$	3.770E−07	1.651E−06	1.554E−07	1.138E−05	1.552E−05
$ErrSQ_{\psi}$	1.236E−10	1.686E−10	2.135E−10	2.421E−10	2.608E−10
$ErrSQ_{\omega}$	2.934E−05	2.885E−05	2.828E−05	2.776E−05	2.733E−05
$ErrSQ_{\bar{u}}$	1.409E−09	2.010E−09	2.749E−09	3.375E−09	3.882E−09
$ErrSQ_{\bar{v}}$	2.580E−09	3.094E−09	3.662E−09	4.178E−09	4.748E−09
$ErrSQ_{\bar{V}}$	3.024E−09	3.491E−09	3.979E−09	4.185E−09	4.354E−09
CPU time(s)	58.861	139.572	412.516	548.677	1609.593

computations, the relative errors decays rapidly with the increase of the computational order, as shown in Fig. 8(a), the absolute error can reach 10^{-9} in a reasonable time, as seen in Fig. 8(b).

It is worth mentioning that the scale of the approximating precision of Coiflets basis in our proposed approach is only dependent on the resolution level j but is irrelevant to the nonlinearity, that is in agreement with Zhao's conclusion [41] for the traditional elementary function basis. The absolute error *ErrSQ* in Fig. 8(b) reduces to a stable level, namely,

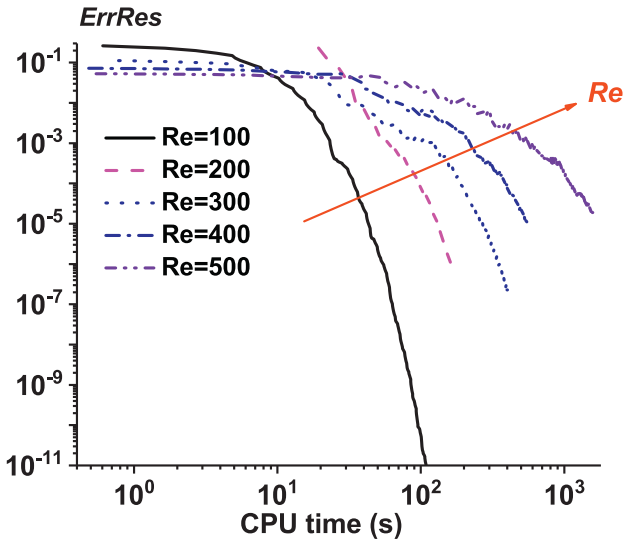

(a) $ErrRes$ of ψ.

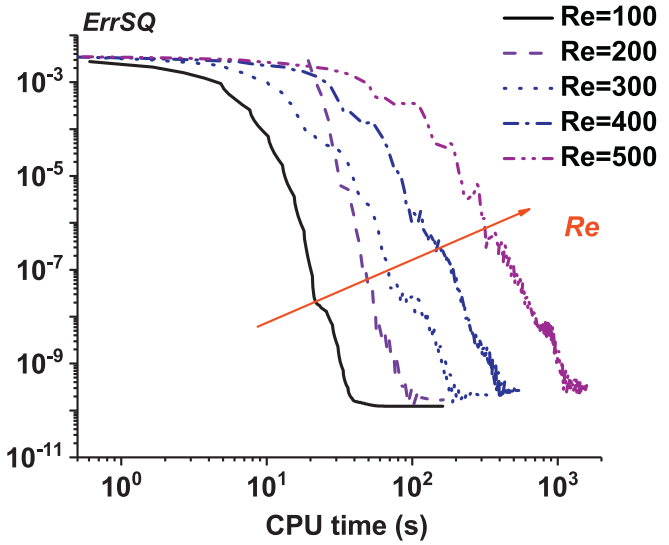

(b) $ErrSQ$ of ψ.

Fig. 8. Convergence process of ψ revealed by *ErrSQ* and *ErrRes* with different Reynolds when $j = 5$.

the approximate scale of 10^{-10} for all Reynolds. But the iteration rate becomes slow as Reynolds increase, that means more iterations are needed to get specific error values in advance.

4.4. Classical problem with singularities

As discussed above, investigations of previous case with exact solution show excellence computational efficiency of our proposed technique, we therefore apply it to the classical cavity flow problem in higher Reynolds with the uniform velocity of the lid-driven being $\bar{U}_0 = f(x) = 1$ in Eq. (61).

It needs to be emphasized that the rigid points (0,1) and (1,1) are singular so that the velocity at such points is not continuous. In the finite difference method, researchers usually overcome the weakness by setting two small amount called double-node approach as the initial iterating parameters. While in our technique, we adopt alternative technique by the Coiflets, as illustrated below.

Table 6
Results of $\psi_{\min}$ and its location, minimum velocity $u_{\min}$ at $x = 0.5$, minimum and maximin velocity $u_{\min}, u_{\max}$ at $y = 0.5$ and their locations by our approach with $c_0 = -0.93$ and $M = 5$ compared with FVM Results for the classical problem when $Re = 0.01$ and $j = 3 \sim 6$.

Variables	This work ($j = 3$)	This work ($j = 4$)	This work ($j = 5$)	This work ($j = 6$)	FVM [40]
$\psi_{\min}$	−1.00348908E−01	−9.99955300E−02	−9.98857540E−02	−1.00102022E−01	−1.00076220E−01
x($\psi_{\min}$)	0.5	0.5	0.5	0.5	0.5
y($\psi_{\min}$)	0.75	0.75	0.75	0.765625	0.76465
$\bar{u}_{\min}$	−2.06400100E−01	−2.06213767E−01	−2.07842507E−01	−2.07745723E−01	−2.07755600E−01
y($\bar{u}_{\min}$)	0.5	0.5625	0.53125	0.53125	0.53564
$\bar{v}_{\min}$	−0.178655984	−0.183209859	−0.184278844	−0.184397791	−1.84449100E−01
x($\bar{v}_{\min}$)	0.75	0.8125	0.78125	0.796875	0.79053
$\bar{v}_{\max}$	1.78402927E−01	1.83234340E−01	1.84275691E−01	1.84389166E−01	1.84441500E−01
x($\bar{v}_{\max}$)	0.25	0.1875	0.21875	0.203125	0.20947
CPU time	0.15 s	2.53 s	24.58 s	882.5 s	4 d10 h

Table 7
Results of $\psi_{\min}$ and its location, minimum velocity $u_{\min}$ at $x = 0.5$, minimum and maximin velocity $u_{\min}, u_{\max}$ at $y = 0.5$ and their locations by our approach with $c_0 = -0.13$ and $M = 5$ compared with FVM Results for the classical problem when $Re = 10$ and $j = 3 \sim 6$.

Variables	This work ($j = 3$)	This work ($j = 4$)	This work ($j = 5$)	This work ($j = 6$)	FVM [40]
$\psi_{\min}$	−1.00615885E−01	−9.98798280E−02	−9.98112060E−02	−1.00137061E−01	−1.00113200E−01
x($\psi_{\min}$)	0.5	0.5	0.53125	0.515625	0.5166
y($\psi_{\min}$)	0.75	0.75	0.75	0.765625	0.76465
$\bar{u}_{\min}$	−2.06453858E−01	−2.05789736E−01	−2.07661250E−01	−2.07584378E−01	−2.07576500E−01
y($\bar{u}_{\min}$)	0.5	0.5625	0.53125	0.53125	0.53467
$\bar{v}_{\min}$	−1.86115119E−01	−1.88362645E−01	−1.88080766E−01	−1.88548241E−01	−1.88506200E−01
x($\bar{v}_{\min}$)	0.75	0.8125	0.78125	0.796875	0.79346
$\bar{v}_{\max}$	1.74023330E−01	1.78530003E−01	1.80858390E−01	1.80869000E−01	1.80911700E−01
x($\bar{v}_{\max}$)	0.25	0.1875	0.21875	0.21875	0.2124
CPU time	3.50 s	34.80 s	395.88 s	5558.18 s	9 d1 h

Table 8
Results of $\psi_{\min}$ and its location, minimum velocity $u_{\min}$ at $x = 0.5$, minimum and maximin velocity $u_{\min}, u_{\max}$ at $y = 0.5$ and their locations by our approach with $c_0 = -0.13$ and $M = 5$ compared with FVM Results for the classical problem when $Re = 100$ and $j = 3 \sim 6$.

Variables	This work ($j = 3$)	This work ($j = 4$)	This work ($j = 5$)	This work ($j = 6$)	FVM [40]
$\psi_{\min}$	−1.42369945E−01	−1.05831527E−01	−1.02448567E−01	−1.03384675E−01	−1.03521200E−01
x($\psi_{\min}$)	0.625	0.625	0.625	0.609375	0.61621
y($\psi_{\min}$)	0.625	0.75	0.75	0.734375	0.7373
$\bar{u}_{\min}$	−3.76074920E−01	−2.09524293E−01	−2.10673843E−01	−2.13622584E−01	−2.14041700E−01
y($\bar{u}_{\min}$)	0.25	0.4375	0.46875	0.453125	0.4585
$\bar{v}_{\min}$	−5.94555821E−01	−3.08263479E−01	−2.47750443E−01	−2.53151085E−01	−2.53804000E−01
x($\bar{v}_{\min}$)	0.875	0.875	0.8125	0.8125	0.81006
$\bar{v}_{\max}$	3.33197374E−01	1.88994985E−01	1.75149885E−01	1.79246343E−01	1.79572814E−01
x($\bar{v}_{\max}$)	0.25	0.25	0.25	0.234375	0.23682
CPU time	5.77 s	48.07 s	414.32 s	6906.41 s	2 d9 h

In a rectangular domain, we consider the discontinuous variable η which is the $\bar{m}$ th order derivative of ξ, whose distribution is $f(x)$ at $y = 1$ and $g(x)$ at $x = 0$ with $f(0) \neq g(1)$ at rigid point (0,1). Then the wavelet expansion at (0,1) is

$$\xi(x,y)|_{(x,y)\to(0,1)} \approx f(0)\varphi_{j,0}(y)\varpi_{j,L}(x) + g(1)\varphi_{j,0}(x)\varpi_{j,R}(y). \tag{94}$$

Meanwhile the $\bar{m}$ line of interpolating matrix $\mathbf{P_0}$ corresponding to $h_{j,0}$ is set to zero. Other discontinuous points can be expanded by Coiflets analogous to the same way. Finally, we substitute Eq. (94) into Eq. (79) via applying wavelet Galerkin method, a modification constant in the iterating equation is appeared.

Numerical solutions of Finite Volume Method with 1024×1024 grids by Marchi et al. [40] are considered as a benchmark listed in Tables 6–9. For the minimum ψ and its position in fluid field, the minimum and the maximum $\bar{v}$ at $y = 1/2$, minimum $\bar{u}$ at $x = 1/2$, we compare our results with the benchmark for $Re = 0.01 \sim 1000$ in the cases of $j = 3 \sim 6$, very excellent agreement is found.

In Tables 10 and 11, our results match well by other numerical methods such as FDM, FVM, LBM, Spectral, Wavelet BEM-FEM and LBM at $Re = 100, 400, 1000$, respectively. We notice from these tables that our computational results for the minimum of ψ, the extremum of the velocity and their locations are improved on by increasing the resolution level j. Particularly, comprehensive considering Tables 3 and 11 at $j = 6$, with very few wavelet basis (64×64) to construct grids in Table 3, our results for $Re = 1000$ have four digits are the same as the ones given by the Marchi et al. [40]. But much little consuming time is needed 8h compared to 60h with superior computing efficiency.

Table 9
Results of $\psi_{\min}$ and its location, minimum velocity $u_{\min}$ at $x = 0.5$, minimum and maximin velocity $u_{\min}$, $u_{\max}$ at $y = 0.5$ and their locations by our approach with other authors for the classical problem when $Re = 400, 1000$ and $j = 5 \sim 6$.

Variables		$Re = 400$		$Re = 1000$	
	This work ($j = 5$)	This work ($j = 6$)	FVM [40]	This work($j = 6$)	FVM [40]
c_0	−1/50	−1/50		−5/1000	
M	5	1	–	2	–
$\psi_{\min}$	−1.12946405E−01	−1.12033208E−01	−1.13988870E−01	−1.18950978E−01	−1.18936708E−01
x($\psi_{\min}$)	0.5625	0.5625	0.55371	0.53125	0.53125
y($\psi_{\min}$)	0.59375	0.609375	0.60547	0.5625	0.56543
$\bar{u}_{\min}$	−3.10420215E−01	−3.20310009E−01	−3.28729500E−01	−3.88433359E−01	−3.88572100E−01
y($\bar{u}_{\min}$)	0.25	0.28125	0.27979	0.171875	0.17139
$\bar{v}_{\min}$	−4.49943256E−01	−4.40397416E−01	−4.54058000E−01	−5.28810267E−01	−5.27056000E−01
x($\bar{v}_{\min}$)	0.90625	0.859375	0.86182	0.90625	0.90967
$\bar{v}_{\max}$	2.92993385E−01	2.95306638E−01	3.03832310E−01	3.77733810E−01	3.76947100E−01
x($\bar{v}_{\max}$)	0.21875	0.234375	0.2251	0.171875	0.15771
CPU time	1.18 h	4.31 h	5 d16 h	8.07 h	60 h

Table 10
Results of $\psi_{\min}$ and its locations by our approach at $j = 6$ and other authors for the classical problem when $Re = 100, 400$.

Authors(Method, Time)	$Re = 100$			$Re = 400$		
	$-\psi_{\min}$	x($\psi_{\min}$)	y($\psi_{\min}$)	$-\psi_{\min}$	x($\psi_{\min}$)	y($\psi_{\min}$)
Burggraf (FDM,1966) [43]	0.1022	–	–	0.1017	–	–
Rubin and Khosla (FDM,1977) [23]	0.1034	–	–	–	–	–
Ghia et al. (FDM,1982) [37]	0.103423	0.6172	0.7344	0.113909	0.5547	0.6055
Schreiber and Keller (FDM,1983) [44]	0.10330	0.61667	0.74167	0.11399	0.55714	0.60714
Vanka (FDM,1986) [45]	0.1034	0.6188	0.7375	0.1136	0.5563	0.6000
Nishida and Satofuka (FDM,1992) [46]	0.103506	0.6094	0.7344	–	–	–
Liao (BEM,1992) [30]	0.1054	0.633	0.748	0.1089	0.556	0.633
Hou et al. (LBM,1995) [29]	0.1030	0.6196	0.7373	0.1121	0.5608	0.6078
Wright and Gaskell (FVM,1995) [47]	0.103519	0.6157	0.7378	–	–	–
Barragy and Carey (FEM,1997) [49]	0.10330	–	–	0.11389	–	–
Zhang (FDM,2003) [50]	0.103511	0.617187	0.734375	–	–	–
Gupta and Kalita (FDM,2005) [51]	0.103	0.6125	0.7375	0.113	0.5500	0.6125
Marchi et al. (FVM,2008)[40]	0.1035212	0.61621	0.7373	0.11398887	0.55371	0.60547
This work($j = 6$)	0.1033962151	0.609375	0.734375	0.1123978384	0.5625	0.609375

Table 11
Results of $\psi_{\min}$ and its locations by our approach at $j = 6$ and other authors for the classical problem when $Re = 1000$.

Ref.	$Re = 1000$		
	$-\psi_{\min}$	x($\psi_{\min}$)	y($\psi_{\min}$)
Rubin and Khosla (FDM,1977) [23]	0.114	–	–
Benjamin and Denny (FDM,1979) [24]	0.1193	–	–
Ghia et al. (FDM,1982) [37]	0.117929	0.5313	0.5625
Schreiber and Keller (FDM,1983) [44]	0.11894	0.52857	0.56429
Vanka (FDM,1986) [45]	0.1173	0.5438	0.5625
Nishida and Satofuka (FDM,1992) [46]	0.119004	0.5313	0.5625
Liao (BEM,1992) [30]	0.1092	0.556	0.595
Hou et al. (LBM,1995) [29]	0.1178	0.5333	0.5647
Wright and Gaskell (FVM,1995) [47]	0.118821	0.5308	0.5659
Goyon(FDM,1996) [48]	0.1157	–	–
Barragy and Carey (FEM,1997) [49]	0.118930	–	–
Botella and Peyret (Spectral,1998) [38]	0.1189366	0.5308	0.5652
Zhang (FDM,2003) [50]	0.118806	0.531250	0.562500
Gupta and Kalita (FDM,2005) [51]	0.117	0.5250	0.5625
Erturk et al. (FDM,2005) [52]	0.118942	0.5300	0.5650
Bruneau and Saad (FDM,2006) [39]	0.11892	0.53125	0.56543
Marchi et al. (FDM,2008) [40]	0.118936708	0.53125	0.56543
This work($j = 6$)	0.118950977790111	0.53125	0.5625

As the Reynolds number increases illustrated in Fig. 9(a), the convergent rate gradually becomes slow, owing to the decrease of the optimal convergence control parameter c_0 decreases. More iterations are needed to obtain the exact results. The velocity vectors at $Re = 2000$ is illustrated in Fig. 9(b) well demonstrating two secondary vorticity at the bottom corners. Besides, in Figs. 10–12, velocity profiles in middle section $x = 0.5$ and $y = 0.5$ of our results at $j = 6$ agree well with benchmark of FVM by Marchi et al. [40], FDM by Ghia et al. [37] and wavelet BEM-FEM by Ravnik et al. [34] with excellent accuracies.

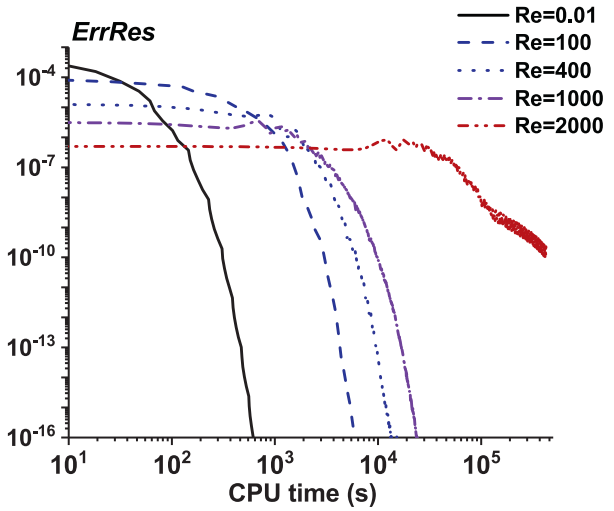

(a) Iterating process revealed by $ErrRes$ with $Re = 0.01 \sim 2000$.

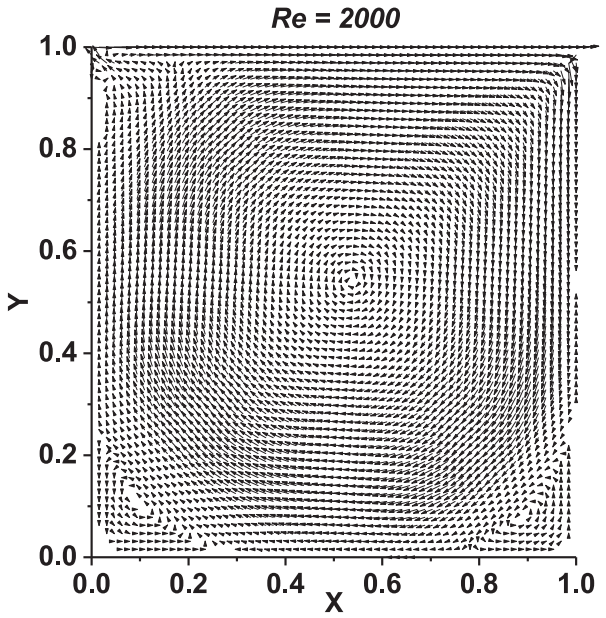

(b) Diagram of Velocity vectors at $Re = 2000$.

Fig. 9. Iterating process when $Re = 0.01 \sim 2000$ and velocity vector at $Re = 2000$.

The vortex induced by the stream-function Eq. (60) near the rigid points (0,1) and (1,1) is unable to be given by the finite difference method due to the discontinuity of velocity on the boundaries. While, we are able to give its distribution near the boundaries, which perfectly matches the results at $Re = 100, 400, 1000$ given by Ghia et al. [37], as shown in Fig. 13. We also notice the accuracies for the vortex distribution at (0,1) and (1,1) can be improved on dramatically by enlarging j.

Actually it is true that the Coiflets applied in our approach possess finite regularity $N = 6$ because of the vanishing moment. Therefore, we are able to approach a function which regularity is less than 6. In this problem, $\psi \in [0, 1]^2$ is continuous in the whole domain but is not derivable on the rigid points. Gibb's phenomenon is inevitable for approaching the velocity field by applying the Coiflets as basis in our method. Finally, we capture more details of vortex on the bound-

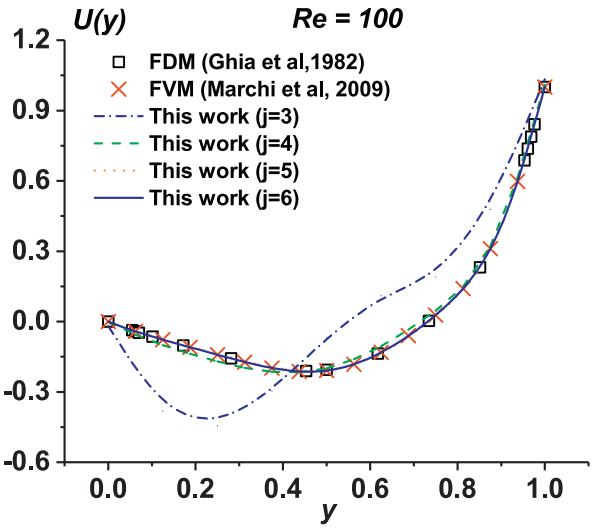

(a) $\bar{u}$ at $x = 1/2$.

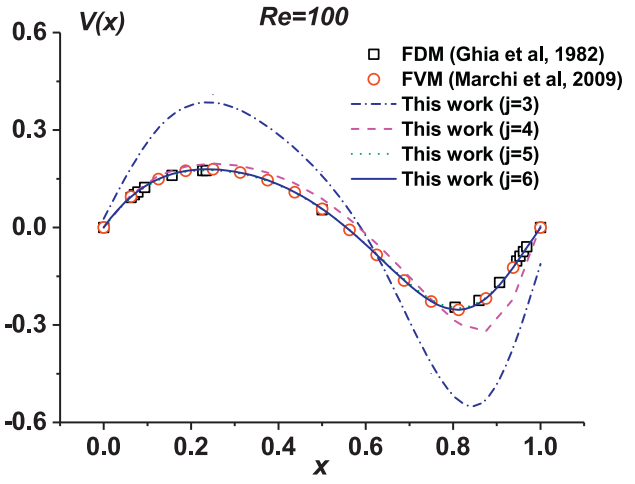

(b) $\bar{v}$ at $y = 1/2$.

Fig. 10. Comparison of $\bar{u}$ at $x = 1/2$ and $\bar{v}$ at $y = 1/2$ when $Re = 100$ with benchmark by FDM (Ghia et al. [37]) and FVM (Marchi et al. [40]).

aries, which show superiority of our approach in application of problems subjected to the incompatible nonhomogeneous boundary conditions.

Certainly, our method is not universal and has its weakness. Theoretically, the increase of the wavelet resolution level can improve on the accuracy of the wavelet solutions. But the larger Reynolds for lid cavity flow needs larger resolution level j since that $Re = 0.01 - 100$ for $j \geq 3$, $Re = 400$ for $j \geq 5$, and $Re = 1000 - 2000$ for $j \geq 6$. Meanwhile, the convergence rate is gradually reduced in Fig. 9(a) for larger Re. The convergence control parameter is adjusted from $-93/100$ at $Re = 0.01$ to $-8/10000$ at $Re = 2000$ to give convergent solutions. To obtain solution for larger $Re > 2000$, we should add j and more iterations. But the calculation condition is not adequate in a desktop with only 8 GB memory, due to the restriction of current computing conditions since it is very time-consuming in Fig. 9(a) (For $Re = 2000$, about 80 h is needed).

In our previous work of solving the same problem by BEM in [30] for $Re = 1 \sim 2000$. By employing the parallel computation in [31], the convergent numerical results for high Reynolds number at $Re = 1 \sim 10000$ are obtained. Similar to the above, further research is needed by applying the parallel computation [31] and introduce new algorithm to accelerate the convergence.

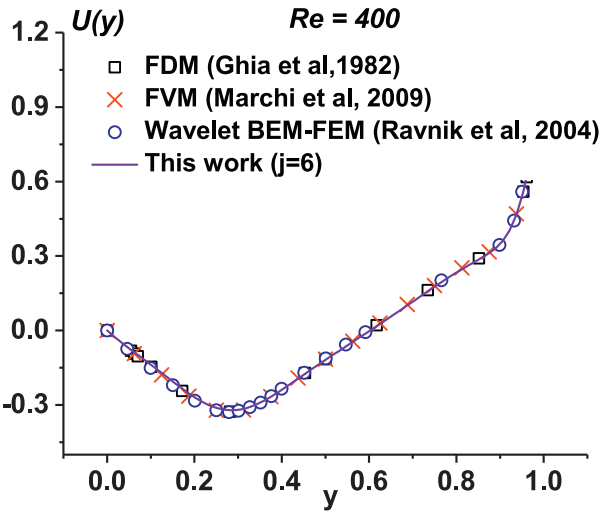

(a) $\bar{u}$ at $x = 1/2$.

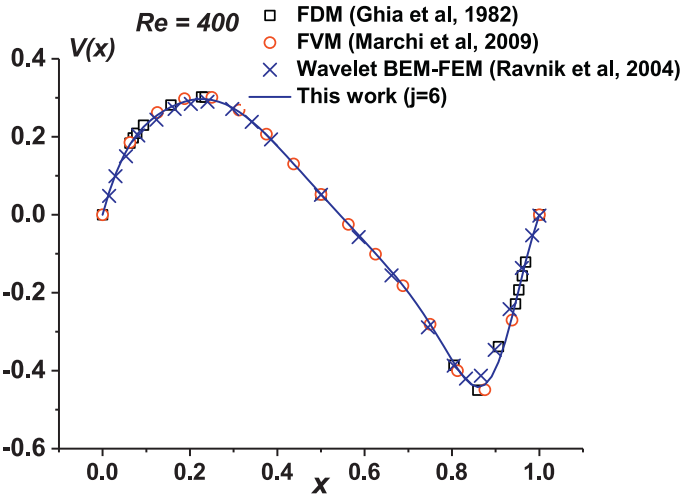

(b) $\bar{v}$ at $y = 1/2$.

Fig. 11. Comparison of $\bar{u}$ at $x = 1/2$ and $\bar{v}$ at $y = 1/2$ when $Re = 400$ with benchmark by FDM (Ghia et al. [37]), Wavelet BEM-FEM (Ravnik et al. [32]) and FVM (Marchi et al. [40]).

5. Conclusions

In the paper, the homotopy-wavelet approach is developed for solving nonhomogeneous boundary value problems, especially for solving the classical laminar flow inside a square cavity. We modify Coiflets by interpolating on the boundaries to construct the boundary Coiflets for linear boundary conditions of Dirichlet, Neumann, and Robin. Further to check the validity and correctness of our proposed technique, we solve the lid-driven cavity flow problem in two cases. One is a validation case with a known analytical solution, another is a case with the up lid moving at a constant velocity with unknown analytical solution in $Re = 0.01 \sim 2000$. Here are the advantages of our approach,

- By introducing boundary wavelets, our approach successfully overcomes the weakness of Liu's wavelet approach [8] and shows great priority. Our approach performs better precision without finding optimal auxiliary homogeneous functions in 1-D linear boundary value problem(BVP). For 2-D BVPs with nonhomogeneous Neumann boundary conditions, our technique also goes well without introducing homogeneous functions. Because it is hardly to find or nonexistent, and Liu's approach does not work in the case.

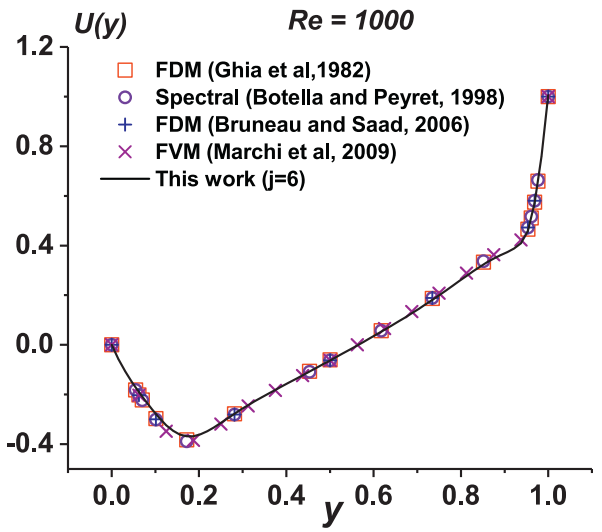

(a) $\bar{u}$ at $x = 1/2$.

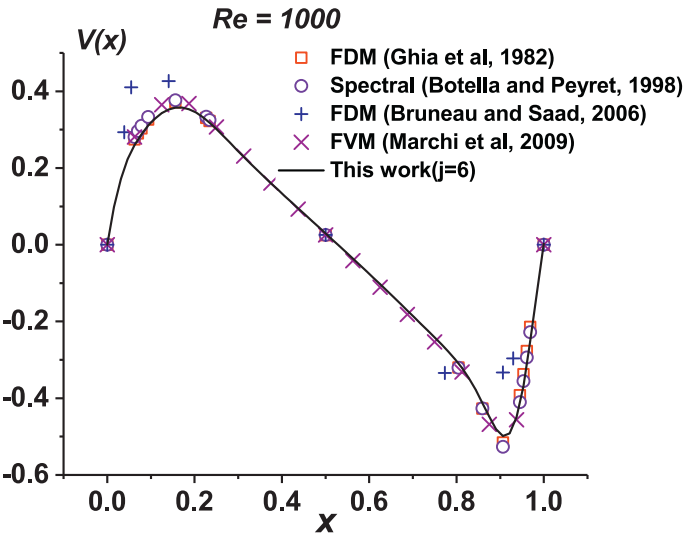

(b) $\bar{v}$ at $y = 1/2$.

Fig. 12. Comparison of $\bar{u}$ at $x = 1/2$ and $\bar{v}$ at $y = 1/2$ when $Re = 1000$ with benchmark by FDM (Ghia et al. [37]), Spectral method (Botella and Peyret [38]), FDM (Bruneau and Saad [39]) and FVM (Marchi et al. [40]).

- For both linear differential equations governed by either Laplace or biharmonic operators, our directly expanded technique via modifying the Coiflets shows good precision and works well for both Cauchy and Neumann boundary conditions.
- We first conduct a preliminary study applying our method in fluid mechanics. In the problem of classical lid driven cavity flow, with very few wavelet basis (64×64) in Table 3, accurate wavelet solutions are obtained with good computing efficiency in comparison with analytical solutions and benchmark by other numerical methods such as FVM, FEM, FDM, LBM, Spectral, Wavelet BEM-FEM. A special strategy is proposed to overcome the singularities on rigid points.

Acknowledgement

Thanks to the anonymous reviewer for their constructive comments and suggestions. This work is partially supported by the National Natural Science Foundation of China (Grant Nos. 11272209 and 11432009).

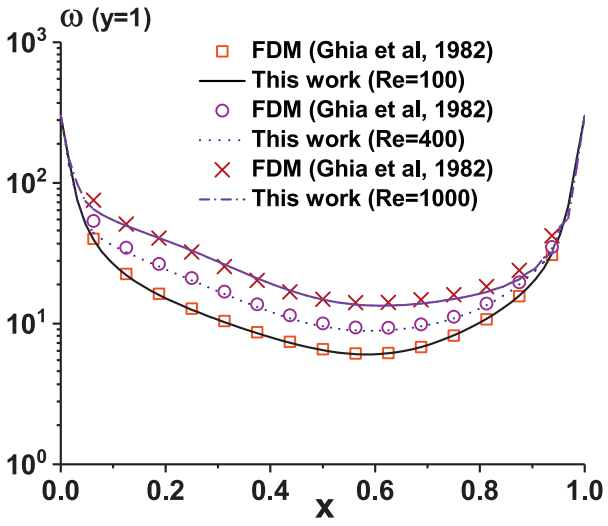

Fig. 13. Vortex distribution near up moving lid ($y = 1$) when $Re = 100, 400, 1000$ at $j = 6$ compared with FDM (Ghia et al. [37]) results.

Appendix A. Some symbolic definitions

Definition 1 (Straight Vector) If Matrix $\mathbf{A} = \{a_{k,l}\}_{m\times n} \in \mathbb{R}^{m\times n}$, then its horizontal straight vector $\hat{\mathbf{A}}$ and vertical straight vector $\check{\mathbf{A}}$ are defined

$$\hat{\mathbf{A}} = \{c_r\}_{mn\times 1} \quad a_{k,l} = c_{l+(k-1)m}, \tag{A.1}$$

$$\check{\mathbf{A}} = \{c_r\}_{mn\times 1} \quad a_{k,l} = c_{k+(l-1)m}. \tag{A.2}$$

Definition 2 (Hadamard/Schur Product) If Matrix $\mathbf{A} = \{a_{k,l}\}_{m\times n}$ and $\mathbf{B} = \{b_{k,l}\}_{m\times n} \in \mathbb{R}^{m\times n}$ (vectors when $m = 1$ and $n = 1$), then their Hadamard/Schur Product $\odot$ is defined

$$\mathbf{A} \bigodot \mathbf{B} = \{c_{k,l} = a_{k,l}b_{k,l}\}_{m\times n}. \tag{A.3}$$

Definition 3 (Kronecker Tensor Product) If Matrix $\mathbf{A} = \{a_{k,l}\}_{m\times n}$ and $\mathbf{B} = \{b_{k,l}\}_{p\times q} \in \mathbb{R}^{p\times q}$ (vectors when $m = 1$ and $n = 1$), then their Kronecker Tensor Product $\bigotimes$ is defined

$$\mathbf{A} \bigotimes \mathbf{B} = \{a_{k,l}\mathbf{B}\}_{mp\times nq}. \tag{A.4}$$

Definition 4 (Dot Product) If Matrix $\mathbf{A} = \{a_{k,l}\}_{m\times n} \in \mathbb{R}^{m\times n}$ is a tensor product, as expressed $\tilde{\mathbf{A}}$. $\hat{\mathbf{B}} = \{b_k\}_{n\times 1} \in \mathbb{R}^{n\times 1}$ is straight vector of matrix $\mathbf{B} = \{b_{k,l}\}_{p\times q} \in \mathbb{R}^{p\times q}$ while $n = pq$, then their matrix product $\bullet$ is emphasized

$$\tilde{\mathbf{A}} \bullet \hat{\mathbf{B}} = \{a_{k,l}b_k\}_{m\times 1}. \tag{A.5}$$

Lemma. If an arbitrary binary $G(x, y) \in L^2([0, 1] \times [0, 1]) \bigcap C^N([0, 1] \times [0, 1])$, then the resolution and reconstitution accuracy [4] of Eqs. (73)–(77) are estimated as

$$\left\| \frac{\partial^{u+v} G(x,y)}{\partial x^u \partial y^v} - \frac{\partial^{u+v} P^j G(x,y)}{\partial x^u \partial y^v} \right\|_{L^2} \le C_p 2^{-j(N-u-v)}, \tag{A.6}$$

$$\left\| \frac{\partial^{u+v} G(x,y)}{\partial x^u \partial y^v} - \frac{\partial^{u+v} S^J G(x,y)}{\partial x^u \partial y^v} \right\|_{L^2} \le C_s 2^{-J(N-u-v)}, \tag{A.7}$$

where C_p and C_s are positive constants that depend only on the function $f(x)$ and wavelets, and $0 \le u + v < N$.

In the generalized orthogonal Coiflets system, the resolution wavelet $h_{j,k}$ and the reconstitution wavelet $h_{J,k}$ are identical. $\hat{\mathbf{G}}$ is the straight vector of the point value of $G(x, y)$ and the elements are coefficients of the Coiflets series used for estimation of its derivatives' vector $\hat{\mathbf{G}}^j_{u,v}$ via Eq. (A.8) with the tensors expressed by resolution wavelet $h_{j,k}$.

Besides, the physical quantities expressed by $G(x, y)$ and its derivatives are reconstituted via Eq. (A.9) with the tensors expressed by reconstitution wavelet $h_{J,k}$.

$$\hat{\mathbf{G}}^j_{u,v} = \tilde{\mathbf{\Pi}}^j_{u,v} \bullet \hat{\mathbf{G}} = \left(\tilde{\mathbf{\Phi}}^j_u \bigotimes \tilde{\mathbf{\Phi}}^j_v\right)^T \bullet \hat{\mathbf{G}}, \tag{A.8}$$

$$\hat{\mathbf{G}}^J_{u,v} = \tilde{\mathbf{\Pi}}^J_{u,v} \bullet \hat{\mathbf{G}} = \left(\tilde{\mathbf{\Phi}}^J_u \bigotimes \tilde{\mathbf{\Phi}}^J_v\right)^T \bullet \hat{\mathbf{G}}. \tag{A.9}$$

where the straight vectors of the point value and the tensors are

$$\widetilde{\mathbf{\Phi}}_u^j = \widetilde{\mathbf{\Phi}}_u^J = \left\{ a_{k,s}^j = a_{k,s}^J = h_{j,k}^{(u)}\left(\frac{s}{2^j}\right)\right\}, \quad \hat{\mathbf{G}} = \left\{ g_o = G\left(\frac{k}{2^j}, \frac{l}{2^j}\right)\right\},$$

$$\hat{\mathbf{G}}_{u,v}^j = \hat{\mathbf{G}}_{u,v}^J = \left\{ g_p^j = g_p^J = \frac{\partial^{u+v}}{\partial x^u \partial y^v} G\left(\frac{s}{2^j}, \frac{t}{2^J}\right)\right\},$$

$$o = 2^j k + l + 1, p = 2^j s + t + 1, \quad k, l, s, t = 0 \sim 2^j.$$

References

[1] Qian S, Weiss J. Wavelets and the numerical solution of boundary value problems. Appl Math Lett 1993;6(1):47–52.
[2] Candela VF. Computation of shift operators in orthonormal compactly supported wavelet bases. SIAM J Numer Anal 1994;31(3):768–87.
[3] Sweldens W, Piessens R. Quadrature formulae and asymptotic error expansions for wavelet approximations of smooth functions. SIAM J Numer Anal 1995;31(4):1240–64.
[4] Tian J. The mathematical theory and applications of biorthogonal Coifman wavelet systems. Ph.D. thesis. Rice University; 1996.
[5] Wei D. Coiflet-type wavelets: theory, design, and applications. The University of Texas at Austin; 1998. Ph.D. thesis.
[6] Zhang L, Liu X, Zhou Y, Wang J. Influence of vanishing moments on the accuracy of a modified wavelet Galerkin method for nonlinear boundary value problems. In: Proceedings of the AIP Conference, 1558; 2013. p. 942–5.
[7] Wang JZ. Generalized theory and arithmetic of orthogonal wavelets and applications to researches of mechanics including piezoelectric smart structures. Ph.D thesis. Lanzhou University; 2001.
[8] Liu X, Zhou Y, Wang X, Wang J. A wavelet method for solving a class of nonlinear boundary value problems. Commun Nonlinear Sci Numer Simul 2013;18(8):1939–48.
[9] Wang J, Zhou Y, Gao H. Computation of the laplace inverse transform by application of the wavelet theory. Commun Numer Methods Eng 2003;19(12):959–75.
[10] Kong L, Wong JSW. Positive solutions for higher order multi-point boundary value problems with nonhomogeneous boundary conditions. J Math Anal Appl 2010;367(2):588–611.
[11] Xie D, Liu Y, Bai C. Existence of multiple positive solutions of higher order multi-point nonhomogeneous boundary value problem. Electr J Qual Theory Differ Equ 2010;33:1–13.
[12] Yang Z, Liao S. A ham-based wavelet approach for nonlinear ordinary differential equations. Commun Nonlinear Sci Numer Simul 2017;48:439–53.
[13] Yang Z, Liao S. A ham-based wavelet approach for nonlinear partial differential equations: two dimensional Bratu problem as an application. Commun Nonlinear Sci Numer Simul 2017;53:249–62.
[14] Yu Q, Xu H, Liao S. Coiflets solutions for föppl-von kármán equations governing large deflection of a thin flat plate by a novel wavelet-homotopy approach. Numer Algorithms 2018;1:1–28.
[15] Liao SJ. Notes on the homotopy analysis method: some definitions and theorems. Commun Nonlinear Sci Numer Simul 2009;14(4):983–97.
[16] Abbasbandy S. The application of homotopy analysis method to nonlinear equations arising in heat transfer. Phys Lett A 2006;360(1):109–13.
[17] Motsa SS, Sibanda P, Shateyi S. A new spectral-homotopy analysis method for solving a nonlinear second order BVP. Commun Nonlinear Sci Numer Simul 2010;15(9):2293–302.
[18] Rashidi MM, Domairry G, Dinarvand S. Approximate solutions for the burger and regularized long wave equations by means of the homotopy analysis method. Commun Nonlinear Sci Numer Simul 2009;14(3):708–17.
[19] Rashidi MM, Pour SAM. Analytic approximate solutions for unsteady boundary-layer flow and heat transfer due to a stretching sheet by homotopy analysis method. Nonlinear Anal Model Control 2010;15(1):83–95.
[20] Rashidi MM, Pour SAM, Hayat T, Obaidat S. Analytic approximate solutions for steady flow over a rotating disk in porous medium with heat transfer by homotopy analysis method. Comput Fluids 2012;54(8):1–9.
[21] Rashidi MM, Freidoonimehr N, Hosseini A, Bg OA, Hung TK. Homotopy simulation of nanofluid dynamics from a non-linearly stretching isothermal permeable sheet with transpiration. Meccanica 2014;49(2):469–82.
[22] Zhou YH, Wang JZ. Generalized gaussian integral method for calculations of scaling function transform of wavelets and its applications. Acta Mathematica Scientia (Chinese Edition) 1999;19(3):293–300.
[23] Rubin S, Khosla P. Polynomial interpolation methods for viscous flow calculations. J Comput Phys 1977;24(3):217–44.
[24] Benjamin AS, Denny VE. On the convergence of numerical solutions for 2-d flows in a cavity at large re. J Comput Phys 1979;33(3):340–58.
[25] Auteri F, Parolini N, Quartapelle L. Numerical investigation on the stability of singular driven cavity flow. J Comput Phys 2002;183(1):1–25.
[26] Abouhamza A, Pierre R. A neutral stability curve for incompressible flows in a rectangular driven cavity. Math Comput Model 2003;38(1):141–57.
[27] Peng YF, Shiau YH, Hwang RR. Transition in a 2-d lid-driven cavity flow. Comput Fluids 2003;32(3):337–52.
[28] Hayase T, Humphrey JAC, Greif R. A consistently formulated quick scheme for fast and stable convergence using finite-volume iterative calculation procedures. J Comput Phys 1992;98(1):108–18.
[29] Hou S, Zou Q, Chen S, Doolen G, Cogley AC. Simulation of cavity flow by the lattice Boltzmann method. J Comput Phys 1995;118(2):329–47.
[30] Liao SJ. Higher order stream function-vorticity formulation of 2d steady-state Navier–Stokes equations. Int J Numer Methods Fluids 1992;15(5):595–612.
[31] Zhao XY, Liao SJ. A short note on the general boundary element method for viscous flows with high Reynolds number. Int J Numer Methods Fluids 2003;42(42):349–59.
[32] Ravnik J, Skerget L, Hribersek M. The wavelet transform for BEM computational fluid dynamics. Eng Anal Bound Elem 2004;28(11):1303–14.
[33] Ravnik J, Skerget L, Hribersek M. Two-dimensional velocity-vorticity based LES for the solution of natural convection in a differentially heated enclosure by wavelet transform based BEM and FEM. Eng Anal Bound Elem 2006;30(8):671–86.
[34] Ravnik J, Skerget L, Hribersek M, Zunic Z. Numerical simulation of dilute particle laden flows by wavelet BEM-FEM. Comput Methods Appl Mech Eng 2008;197(6–8):789–805.
[35] Auteri F, Quartapelle L. Galerkin spectral method for the vorticity and stream function equations. J Comput Phys 1999;149(149):306–32.
[36] Bruneau CH, Jouron C. An efficient scheme for solving steady incompressible Navier–Stokes equations. J Comput Phys 1990;89(2):389–413.
[37] Ghia U, Ghia KN, Shin CT. High-re solutions for incompressible flow using the Navier–Stokes equations and a multigrid method. J Comput Phys 1982;48(3):387–411.
[38] Botella O, Peyret R. Benchmark spectral results on the lid-driven cavity flow. Comput Fluids 1998;27(4):421–33.
[39] Bruneau CH, Saad M. The 2d lid-driven cavity problem revisited. Comput Fluids 2006;35(3):326–48.
[40] Marchi, Henriquesuero C, RobertaAraki, Kiyoshi L. The lid-driven square cavity flow: numerical solution with a 1024x1024 grid. J Braz Soc Mech Sci and Eng 2009;31(3):186–98.
[41] Zhao Y, Lin Z, Liao S. An iterative ham approach for nonlinear boundary value problems in a semi-infinite domain. Comput Phys Commun 2013;184(9):2136–44.
[42] Kawaguti M. Numerical solution of the Navier–Stokes equations for the flow in a two-dimensional cavity. J Phys Soc Jpn 1961;16(11):2307–15.
[43] Burggraf OR. Analytical and numerical studies of the structure of steady separated flows. J Fluid Mech 1966;24(1):113–51.

[44] Schreiber R, Keller HB. Driven cavity flows by efficient numerical techniques. J Comput Phys 1983;49(2):310–33.
[45] Vanka SP. Block-implicit multigrid solution of Navier–Stokes equations in primitive variables. J Comput Phys 1985;65(1):138–58.
[46] Nishida H, Satofuka N. Higher-order solutions of square driven cavity flow using a variable-order multi-grid method. Int J Numer Methods Eng 2010;34(2):637–53.
[47] Wright NG, Gaskell PH. An efficient multigrid approach to solving highly recirculating flows. Comput Fluids 1995;24(1):63–79.
[48] Goyon O. High-Reynolds number solutions of Navier–Stokes equations using incremental unknowns. Comput Methods Appl Mech Eng 1996;130(3–4):319–35.
[49] Barragy E, Carey GF. Stream function-vorticity driven cavity solution using p finite elements. Comput Fluids 1997;26(5):453–68.
[50] Zhang J. Numerical simulation of 2d square driven cavity using fourth-order compact finite difference schemes. Comput Math Appl 2003;45(1):43–52.
[51] Gupta MM, Kalita JC. A new paradigm for solving Navier–Stokes equations: streamfunction-velocity formulation. J Comput Phys 2005;207(1):52–68.
[52] Erturk E, Corke TC, Gökcöl C. Numerical solutions of 2steady incompressible driven cavity flow at high Reynolds numbers. Int J Numer Methods Fluids 2005;48(48):747–74.